NASA TECHNICAL NOTE

NASA TN D-7060

NASA TN D-7060

EFFECT OF WING SWEEP, ANGLE OF ATTACK, REYNOLDS NUMBER, AND WING ROOT FILLET ON THE INTERFERENCE HEATING TO THE WING WINDWARD SURFACE OF AN ENTRY VEHICLE CONFIGURATION

by Louis E. Clark

Langley Research Center
Hampton, Va. 23365

NATIONAL AERONAUTICS AND SPACE ADMINISTRATION • WASHINGTON, D. C. • DECEMBER 1972

1. Report No.	2. Government Accession No.	3. Recipient's Catalog No.
NASA TN D-7060		

4. Title and Subtitle	5. Report Date
EFFECT OF WING SWEEP, ANGLE OF ATTACK, REYNOLDS NUMBER, AND WING ROOT FILLET ON THE INTERFERENCE HEATING TO THE WING WINDWARD SURFACE OF AN ENTRY VEHICLE CONFIGURATION	December 1972
	6. Performing Organization Code

7. Author(s)	8. Performing Organization Report No.
Louis E. Clark	L-8486
	10. Work Unit No.
9. Performing Organization Name and Address	502-37-01-10
NASA Langley Research Center Hampton, Va. 23365	11. Contract or Grant No.
	13. Type of Report and Period Covered
12. Sponsoring Agency Name and Address	Technical Note
National Aeronautics and Space Administration Washington, D.C. 20546	14. Sponsoring Agency Code

15. Supplementary Notes

16. Abstract

The phase-change-coating technique was used to study the interference heating to the windward surface of 14°, 25°, and 50° swept wings of an entry vehicle configuration. One wing root of each model was faired to the fuselage with a fillet. Tests were made at Mach 8 at angles of attack of 0°, 20°, 40°, and 60° and at free-stream Reynolds numbers based on model length of 0.47×10^6 and 1.7×10^6.

Bow shock impingement heating was found to increase in magnitude and affected area with increasing angle of attack until at a higher angle of attack it decreases; this angle of attack is lower for a 50° swept wing. Wing root interference heating was found to increase with angle of attack up to 40° and then to remain approximately constant. Consequently, wing root interference heating becomes the major type of interference heating at large angles of attack, and this occurs at a lower angle of attack for the highest sweep angle. A wing leading-edge root fillet reduces the peak in wing root interference heating near the leading edge, and increasing Reynolds number increases the level of interference heating.

The total heating to the windward surface of the swept wings was found to increase with increasing angle of attack (up to about 40°) and Reynolds number and to decrease with increasing wing sweep. Transmitted shock impingement position was found to move inboard as angle of attack increased, with variations in rate and distance depending on wing sweep angle.

17. Key Words (Suggested by Author(s))	18. Distribution Statement
Interference heating Entry heating	Unclassified – Unlimited

19. Security Classif. (of this report)	20. Security Classif. (of this page)	21. No. of Pages	22. Price*
Unclassified	Unclassified	52	$3.00

*For sale by the National Technical Information Service, Springfield, Virginia 22151

EFFECT OF WING SWEEP, ANGLE OF ATTACK, REYNOLDS NUMBER, AND WING ROOT FILLET ON THE INTERFERENCE HEATING TO THE WING WINDWARD SURFACE OF AN ENTRY VEHICLE CONFIGURATION

By Louis E. Clark
Langley Research Center

SUMMARY

The phase-change-coating technique was used to study the interference heating to the windward surface of 14°, 25°, and 50° swept wings of an entry vehicle configuration. One wing root of each model was faired to the fuselage with a fillet. Tests were made at Mach 8 at angles of attack of 0°, 20°, 40°, and 60° and at free-stream Reynolds numbers based on model length of 0.47×10^6 and 1.7×10^6.

Bow shock impingement heating was found to increase in magnitude and affected area with increasing angle of attack until at a higher angle of attack it decreases; this angle of attack is lower for a 50° swept wing. Wing root interference heating was found to increase with angle of attack up to 40° and then to remain approximately constant. Consequently, wing root interference heating becomes the major type of interference heating at large angles of attack, and this occurs at a lower angle of attack for the highest sweep angle. A wing leading-edge root fillet reduces the peak in wing root interference heating near the leading edge, and increasing Reynolds number increases the level of interference heating.

The total heating to the windward surface of the swept wings was found to increase with increasing angle of attack (up to about 40°) and Reynolds number and to decrease with increasing wing sweep. Transmitted shock impingement position was found to move inboard as angle of attack increased, with variations in rate and distance depending on wing sweep angle.

INTRODUCTION

Increased heating will occur at the impingement of a bow shock on the wings and in the fuselage-wing intersection region of shuttle vehicles and hypersonic aircraft. Experimental wind-tunnel studies have been conducted (1) to measure the increased heating due to shock impingement on swept leading edges (refs. 1, 2, and 3, for example) and (2) on the heat transfer in the vicinity of a 90° corner alined with the free-stream velocity

(refs. 4 and 5, for example). Investigations of these types of interference heating to the wing windward surface of a fixed-wing orbiter at a single wing sweep angle are reported in references 6 and 7.

There is a need for information on the variation of interference heating over a range of wing leading-edge sweep angle, angle of attack, and Reynolds number and on the effect of a small circular fillet on wing root heating. The present investigation was conducted to determine this information. Three 0.007-scale models of an entry vehicle configuration with wings having 14°, 25°, and 50° sweep were tested at angles of attack of 0°, 20°, 40°, and 60° at Reynolds numbers based on model length of 0.47×10^6 and 1.7×10^6. The wing leading edge on one side of each model was faired to the fuselage with a small circular fillet. The models were tested in the Langley Mach 8 variable-density hypersonic tunnel, and the heat-transfer data were obtained by using the phase-change-coating technique described in reference 8.

SYMBOLS

c_p specific heat

h heat-transfer coefficient

h_{ref} reference heat-transfer coefficient, stagnation-point value for a 0.213-centimeter-radius sphere at test conditions

k thermal conductivity

M_∞ free-stream Mach number

N_{Pr} Prandtl number

$R_{\infty,l}$ Reynolds number based on free-stream conditions and scaled length of model

S wing area having heat-transfer coefficient equal to or greater than given heat-transfer coefficient

S_t total exposed wing planform area

s surface distance along vertical plane of symmetry measured from Newtonian stagnation point

t	time, sec
V	velocity
w	maximum width of model fuselage at wing leading edge
x	axial length of model measured from nose
y	distance along wing span measured from fuselage center line
α	angle of attack
Λ	wing sweep angle
μ	viscosity
ρ	density

Subscripts:

s	stagnation conditions
w	wall conditions

FACILITY

The tests were conducted in the Langley Mach 8 variable-density hypersonic tunnel which is described in reference 9. This facility, which operates with air as the test medium, has a contoured axisymmetric nozzle with a 37.72-centimeter-diameter test section. It is adapted for transient testing by means of a model injection mechanism located beneath the test section. Windows are available on the test section for lighting and photographing the model.

Stagnation pressures for the tests were 0.793 and 3.55 kN/m^2 with corresponding stagnation temperatures of about 710 and 782 K, resulting in Reynolds numbers based on model length of 0.47×10^6 and 1.7×10^6.

MODELS

Three models of an entry vehicle configuration with wing sweep angles of 14^{o}, 25^{o}, and 50^{o} were tested. The wing leading edge on one side of each model was faired to the fuselage with a small circular fillet. Figures 1 and 2 give details of the fuselage and wings, and figure 3 shows details of the model sting configuration. The models were cast from a high-temperature epoxy material. Measurements of the thermophysical properties of the wings gave values of $\sqrt{\rho c_p k}$ from 1.711 to 1.762 W-sec$^{1/2}$/(m^2-K).

TEST TECHNIQUE AND DATA REDUCTION

The phase-change-coating technique described in reference 8 was used to obtain the heat-transfer data. With this technique the time for the surface of the model to reach the phase-change temperature of the thin coating is measured by use of motion-picture photography. These values of time and temperature are used with the solution to the one-dimensional heat-conduction equation to calculate the heat-transfer coefficients. The calculations are based on the assumption that the body geometry can be represented by a semi-infinite slab. This assumption is a good approximation to the actual body geometry when the depth of heat penetration is small compared with pertinent model dimensions. The temperatures of the phase-change material used in the present tests were selected so that the heat-penetration depths remained small enough to satisfy the one-dimensional assumption to within 0.127 centimeter of the wing leading edge. The heat-transfer coefficients for any isotherms within 0.127 centimeter of the leading edge are subject to errors which have been calculated by the method of reference 10 to be about 25 percent at most and are always larger than the actual value. Several tests using different melting temperatures of phase-change material (338 to 477 K) were made as required to obtain complete data.

Data were not taken until 1 second after the model was initially exposed to the flow. Experience has shown this time interval to be sufficiently long to minimize errors caused by erroneous heating rates when the model passes through the tunnel boundary layer and by the uncertainty in initial time.

The data were reduced by using the free-stream total temperature for the adiabatic wall temperature. The data are presented as the ratio h/h_{ref} where h is the experimental value of the heat-transfer coefficient and h_{ref} is the theoretical value at the stagnation point of a 0.213-centimeter-radius sphere. The value of h/h_{ref} was computed by the method of reference 11, in which

$$h_{ref} = 0.768 \frac{c_p}{778} (N_{Pr,w})^{-0.6} (\rho_w \mu_w)^{0.1} (\rho_s \mu_s)^{0.4} \left(\frac{dV}{ds}\right)^{0.5}$$

and $\frac{dV}{ds}$ was calculated by using Newtonian theory.

RESULTS AND DISCUSSION

Peak Heating

Two general types of interference heating are present: (1) increased heating due to impingement of the fuselage bow shock on the wing and (2) increased heating in the region of the wing root due to interference between the fuselage and the wing. Typical phase-change patterns obtained with front-lighted schlieren for the 14°, 25°, and 50° swept wings are shown in figure 4. The models were at a slight yaw angle so that the shocks are not symmetrical. The coating is unmelted in the light areas and the phase change has already occurred in the dark areas due to the higher heating rate. The line separating these areas represents a known temperature and thus a constant heat-transfer coefficient. In the absence of interference heating the isotherms would be essentially parallel to the wing leading edge, and the occurrence of interference heating causes peaks in the isotherms directed toward the trailing edge (see also fig. 6). Bow shock impingement causes the characteristic two-peaked interference pattern which occurs near the wing tips and is pronounced at $\Lambda = 14^\circ$ and 25°. The models are at an angle of attack so that the actual intersection of the bow and wing shocks occurs inboard of the apparent intersection observed in the schlieren photographs. The heating peak near the wing root is due to wing-fuselage interference heating.

Usually the line between the unmelted and melted areas of phase-change paint is easily distinguished; however, at certain combinations of wing sweep and angle of attack, regions occur near the wing roots in which distinct phase-change lines do not occur and, instead, the region gradually turns darker over a period of time. An example is shown in figure 5 for the 25° swept wing at a 40° angle of attack. Note the regions near the wing roots where a gradual darkening occurs between $t = 1$ sec and $t = 4$ sec. This behavior is believed to be caused by the existence of a constant heating rate throughout the region or by shear forces removing the phase-change material. Only the times at which distinct lines occurred are used, which occasionally results in wide spacings between the isotherms. In some cases, the isotherms were estimated and are shown by dashed lines.

Angle of attack.- The peaks of both bow shock impingement heating and wing root interference heating are, in general, much smaller at 0° angle of attack (figs. 6 to 8) at

all sweep angles than the heating peaks which occur at higher angles of attack (figs. 9 to 17). Both types of interference heating peaks increase and the interference area becomes broader on the 14° and 25° swept wings as the angle of attack increases to 40°; but as the angle of attack increases to 60° (figs. 15 and 16) the bow shock impingement peak decreases substantially so that the wing root heating, which remains about constant, is the major type of interference heating. Similar behavior occurs on the 50° swept wing except that the decrease in the bow shock impingement heating peak occurs at a lower angle of attack between 20° and 40° and, as a consequence, wing root heating becomes the major type of interference heating at 40° angle of attack.

Increasing angle of attack causes the location of the bow shock impingement heating peak to move inboard and become more inclined to the fuselage and causes the wing root interference heating to move onto the fuselage.

Some idea of the complexity of the flow patterns existing in the present tests can be gained from reference 12 which analyzes six types of interference heating that occur depending on wing sweep angle and location of the shock intersection. The results of reference 12 are, in general, only applicable to the leading-edge region, but many similar types of interference heating may be expected to occur on the wing windward surface as the wing sweep angle and angle of attack are varied. For example, the change in the bow shock impingement heating pattern from two peaks to one peak on the 50° swept wing as the angle of attack increases from 20° to 40° (figs. 11 and 14) is probably due to a change in the type of interference heating. A limited discussion of the type of interference heating occurring on wing windward surfaces is given in references 6, 7, and 12.

Wing leading-edge sweep.- An inspection of figures 6 to 17 shows that, in general, the magnitude and area involved of both the wing root interference heating and bow shock impingement heating peaks are similar on the 14° and 25° swept wings and that as wing sweep increases to 50° a decrease occurs in both types of interference heating peaks. Increasing wing sweep also reduces the tendency of the wing root heating peak to move onto the fuselage as the angle of attack increases. An exception to the general trend of decreasing interference heating at a 50° sweep angle occurs at 60° angle of attack at $R_{\infty,l}$ of 1.7×10^6 (fig. 17(b)). At these conditions the heating peak due to bow shock impingement is more pronounced on the 50° swept wing than on the 14° and 25° swept wings.

Wing root fillet.- The general effect of the leading-edge wing root fillet over the range of angle of attack, wing sweep, and Reynolds number (figs. 6 to 17) is to reduce the heating peaks in the wing root interference near the leading edge.

Reynolds number.- The effect of increasing $R_{\infty,l}$ from 0.47×10^6 to 1.7×10^6 in most cases is to increase the heating peaks due to both bow shock impingement and wing

root interference, an indication of more severe interference heating, and to begin to move the wing root interference heating peak onto the fuselage at the midchord location.

Fuselage heating.- Except for differences in scale, the fuselage of the models tested in reference 6 is identical to that of the models used in the present tests. The heating along the windward surface of this fuselage is reported in reference 6 and is not repeated herein. The results reported in reference 6 on a 16° swept wing agree well with the 14° swept wing of the present tests.

Total Heating to the Wing Windward Surface

In order to illustrate the effect of the various parameters on the total heating to the wing windward planform, the fractional wing area with a heat-transfer coefficient equal to or greater than a given heat-transfer coefficient was calculated. The effects of angle of attack, wing sweep, wing root fillet, and Reynolds number on this parameter are discussed in the following sections.

Angle of attack.- The highest heat-transfer coefficients occur near the wing leading edge and decrease until a minimum is reached at the trailing edge (fig. 18). The heat-transfer coefficients increase with angle of attack over most of the wing surface at all sweep angles (fig. 18); however, this trend reverses near the leading edge. As a consequence, the total heating to the wing increases with angle of attack until the decreasing heat transfer at the front of the wing offsets the increase which occurs farther back. This occurs at an angle of attack of 40°, and the total heating to the wing remains about constant or decreases slightly as the angle of attack is increased to 60°. The trend is most apparent on the 50° swept wing (fig. 18(c)).

The heating changes observed with increasing angle of attack are caused by dual effects: (1) an increase in heat transfer over most of the wing as the surface flow approaches stagnation conditions and (2) the initial increase and then decrease of bow shock impingement heating peak with angle of attack. The causes for the changes in total heating are difficult to isolate because of these interacting mechanisms, but the leveling off of the total wing heating at angles of attack between 40° and 60° is probably largely due to the substantial decrease in the bow shock impingement heating peak which occurs in this range.

Wing leading-edge sweep.- The effect of increasing wing leading-edge sweep is a moderate decrease in the total heating to the wing windward surface over the angle-of-attack range (fig. 19). The bumps present in some of the curves are probably due to inaccuracies in reducing the data. An exception to the trend occurs at a $R_{\infty,l}$ of 1.7×10^6 and an angle of attack of 20° but is not shown in the figures. At these conditions the total heating to the 25° swept wing exceeds that to the 14° swept wing.

Wing root fillet.- The leading-edge root fillet not only decreases the wing root interference heating peak near the leading edge, but for most of the conditions shown in figure 20 it also slightly reduces the average heat-transfer coefficient along the wing chord. A number of exceptions to this general trend occurred, including the 14° swept wing at an angle of attack of 60° at both Reynolds numbers and the 25° and 50° swept wings at angles of attack of 60° and 40°, respectively, at the higher Reynolds number.

Reynolds number.- The nature of the boundary layer in the interference region is unknown, but it is probably laminar since the highest Reynolds number based on leading-edge diameter is more than an order of magnitude below the transition data reported in the survey of reference 13 and the present heating data do not exhibit the increase with distance along the wing which would occur during transition. Based on the assumption that the boundary layer is laminar, nondimensionalizing the heat-transfer coefficients at each Reynolds number by their respective laminar reference heat-transfer coefficients (fig. 21) eliminates increases due solely to increased Reynolds number and the differences observed are due only to changes in the interference heating. Increasing Reynolds number usually results in higher average heat-transfer coefficients and increased total heating, particularly at the higher angles of attack, but at angles of attack of 0° and 20° the total heating to the 14° swept wing appears to decrease with increasing Reynolds number. The trend of increased total interference heating with increasing Reynolds number also occurred on the wing with the root fillet.

Transmitted Shock Impingement Point on the Wing Leading Edge

The shock impingement point (fig. 22) was located at angles of attack up to 40° by extrapolating along the inboard peak of the typical two-peaked interference pattern to the leading edge. The small peak in the isotherms near the leading edge at an angle of attack of 60° (fig. 16) was extrapolated to the leading edge and taken as the impingement location. Bow shock impingement did not occur on the 50° swept wing at 0° angle of attack and its position on a wing of longer span was estimated from the bow shock angle.

The impingement point on the 14° and 25° swept wings moves inboard as the angle of attack increases to about 30°, remains almost constant from 30° to 50°, and moves slightly inboard as the angle of attack increases to 60°. In contrast, the impingement point on the 50° swept wing continually moves inboard as the angle of attack increases to 60°. No consistent change in impingement point is apparent when the Reynolds number $R_{\infty,l}$ is varied from 0.47×10^6 to 1.7×10^6.

CONCLUSIONS

An investigation of bow shock impingement heating and wing root interference heating to the wing windward surface was conducted at Mach 8 for wing sweep angles of 14°, 25°, and 50° at angles of attack of 0°, 20°, 40°, and 60° and at free-stream Reynolds numbers based on model length of 0.47×10^6 and 1.7×10^6. Measurements obtained lead to the following conclusions:

1. The heating peaks due to bow shock impingement and wing root interference were found to be similar on the 14° and 25° swept wings and to decrease as the wing sweep increased to 50°.

2. The bow shock impingement heating initially increases and the interference area becomes broader as the angle of attack increases until at some higher angle of attack it decreases; this angle of attack is lower for the 50° swept wing. The wing root interference heating increases with angle of attack up to 40° and then remains approximately constant for all sweep angles. As a result, at large angles of attack the wing root interference heating becomes the dominant type of interference heating. The angle of attack at which this occurs varies with sweep angle, being lower for the largest sweep angle.

3. A small circular fillet of the wing leading edge was found to reduce the peak in the wing root interference heating near the leading edge.

4. With increasing Reynolds number both types of heating peaks increased and the wing root interference heating began to move onto the fuselage.

5. The total heating to the wing windward surface was found to increase with angle of attack up to about 40° and then to remain approximately constant for all sweep angles as the angle of attack increased to 60°. The total interference heating also increased with increasing Reynolds number and decreased with increasing leading-edge sweep.

6. Transmitted shock impingement position was found to move inboard as the angle of attack increased, with variations in rate and distance depending on wing sweep angle.

Langley Research Center,
National Aeronautics and Space Administration,
Hampton, Va., November 16, 1972.

REFERENCES

1. Beckwith, Ivan E.: Experimental Investigation of Heat Transfer and Pressures on a Swept Cylinder in the Vicinity of Its Intersection With a Wedge and Flat Plate at Mach Number 4.15 and High Reynolds Numbers. NASA TN D-2020, 1964.

2. Bushnell, Dennis M.: Interference Heating on a Swept Cylinder in Region of Intersection With a Wedge at Mach Number 8. NASA TN D-3094, 1965.

3. Hiers, Robert S.; and Loubsky, William J.: Effects of Shock-Wave Impingement on the Heat Transfer on a Cylindrical Leading Edge. NASA TN D-3859, 1967.

4. Stainback, P. Calvin: Heat-Transfer Measurements at a Mach Number of 8 in the Vicinity of a 90° Interior Corner Alined With the Free-Stream Velocity. NASA TN D-2417, 1964.

5. Watson, Ralph D.; and Weinstein, Leonard M.: A Study of Hypersonic Corner Flow Interactions. AIAA Paper No. 70-227, Jan. 1970.

6. Hunt, James L.; and Jones, Robert A.: Heating and Flow-Field Studies on a Straight-Wing Hypersonic Reentry Vehicle at Angles of Attack From 20° to 80° With Simulation of Real-Gas Trends. NASA TN D-7108, 1973.

7. Seegmiller, H. Lee: Shock Interference Heating and Density-Ratio Effects. Part I – Flow Field Visualization, Thermocouple Measurements, and Analysis. NASA Space Shuttle Technology Conference, Vol. I, NASA TM X-2272, 1971, pp. 185-215.

8. Jones, Robert A.; and Hunt, James L.: Use of Fusible Temperature Indicators for Obtaining Quantitative Aerodynamic Heat-Transfer Data. NASA TR R-230, 1966.

9. Schaefer, William T., Jr.: Characteristics of Major Active Wind Tunnels at the Langley Research Center. NASA TM X-1130, 1965.

10. Hunt, James L.; and Pitts, Joan I.: Thin Wing Corrections for Phase-Change Heat-Transfer Data. J. Spacecraft & Rockets, vol. 8, no. 12, Dec. 1971, pp. 1228-1230.

11. Fay, J. A.; and Riddell, F. R.: Theory of Stagnation Point Heat Transfer in Dissociated Air. J. Aeronaut. Sci., vol. 25, no. 2, Feb. 1958, pp. 73-85, 121.

12. Edney, Barry: Anomalous Heat Transfer and Pressure Distributions on Blunt Bodies at Hypersonic Speeds in the Presence of an Impinging Shock. FFA Rep. 115, Aeronaut. Res. Inst. of Sweden, 1968.

13. Bushnell, Dennis M.; and Huffman, Jarrett K.: Investigation of Heat Transfer to Leading Edge of a 76° Swept Fin With and Without Chordwise Slots and Correlations of Swept-Leading-Edge Transition Data for Mach 2 to 8. NASA TM X-1475, 1967.

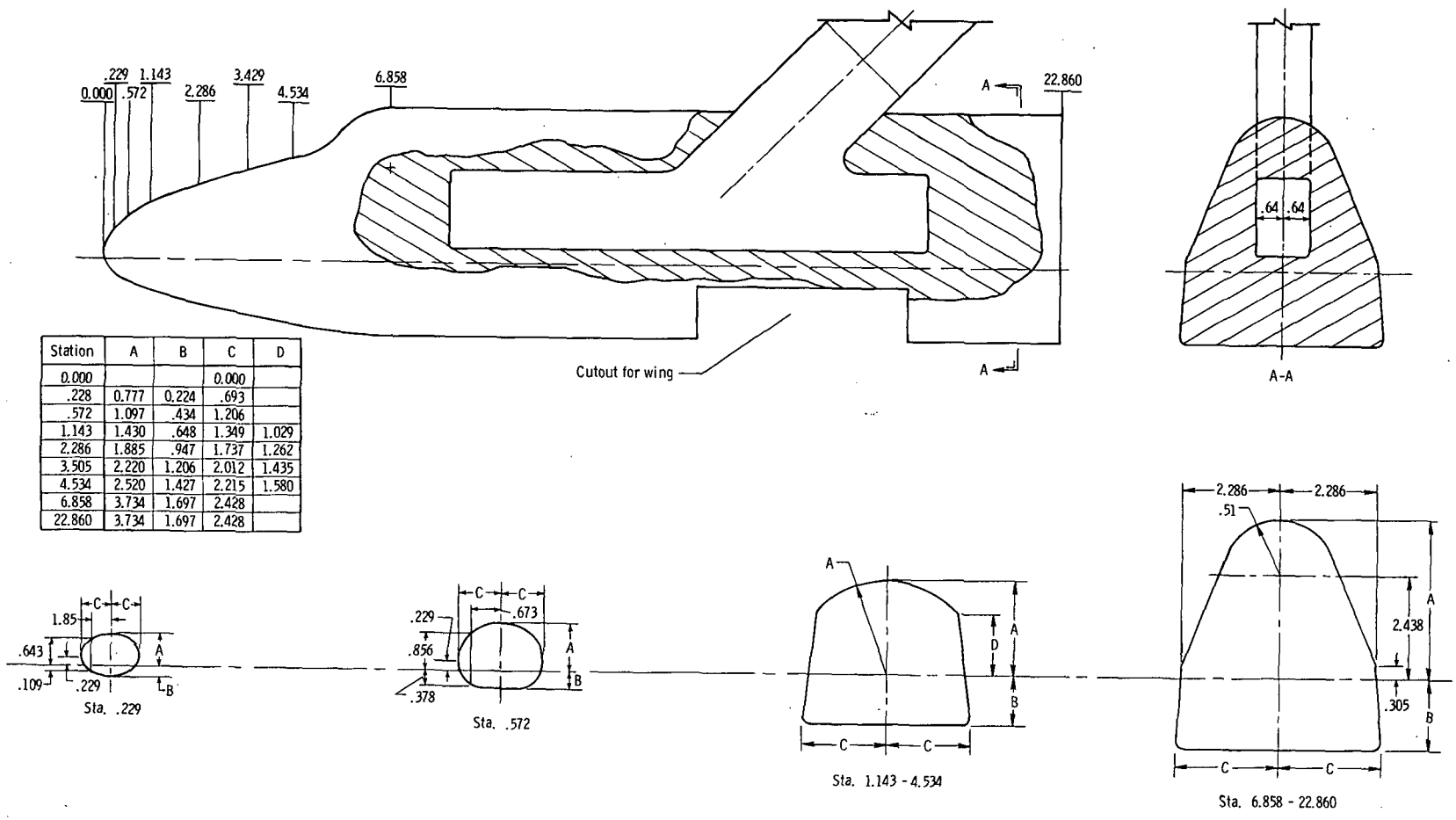

Station	A	B	C	D
0.000			0.000	
.228	0.777	0.224	.693	
.572	1.097	.434	1.206	
1.143	1.430	.648	1.349	1.029
2.286	1.885	.947	1.737	1.262
3.505	2.220	1.206	2.012	1.435
4.534	2.520	1.427	2.215	1.580
6.858	3.734	1.697	2.428	
22.860	3.734	1.697	2.428	

Figure 1.- Fuselage coordinates. All dimensions are in centimeters.

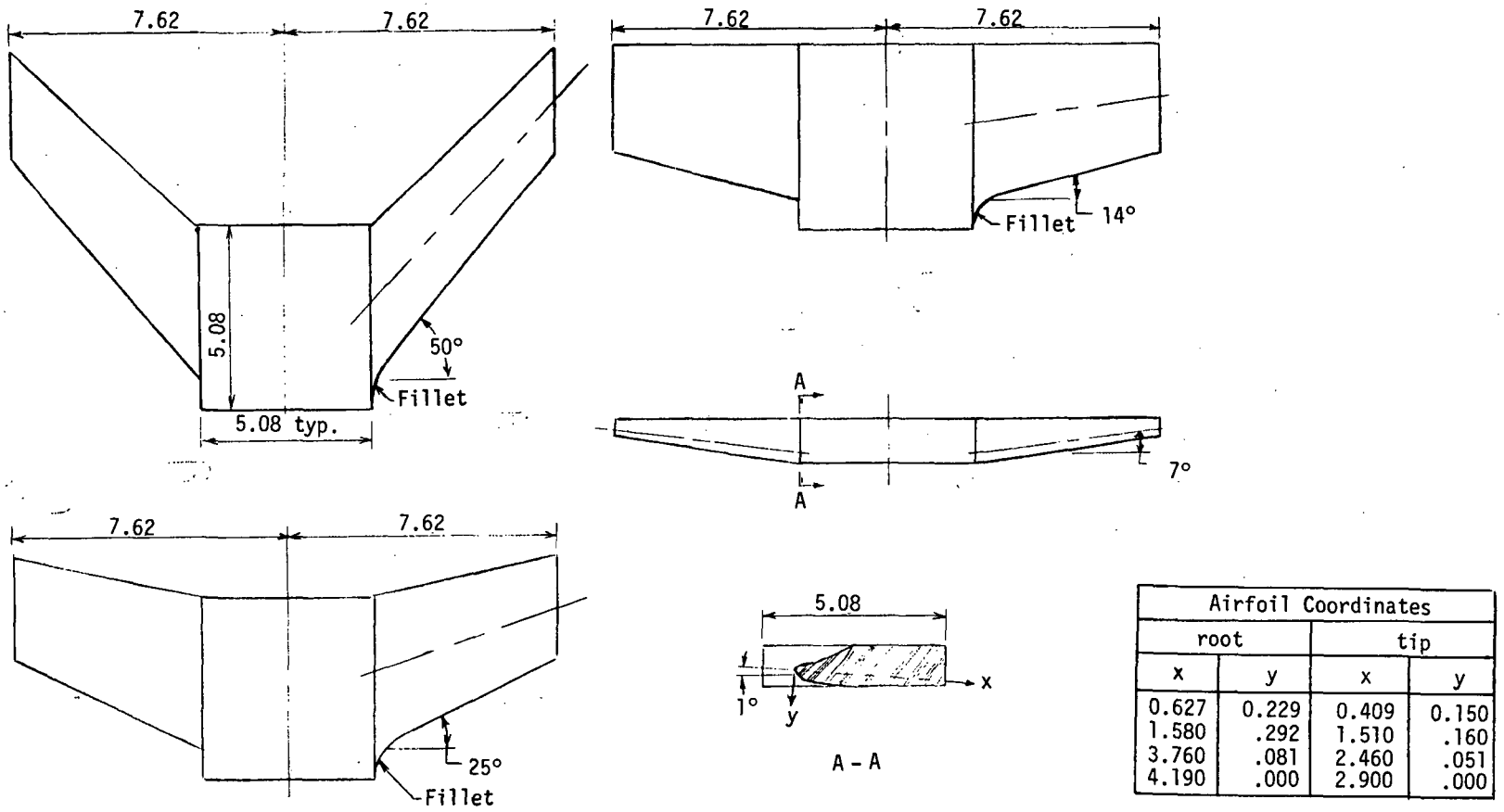

Airfoil Coordinates			
root		tip	
x	y	x	y
0.627	0.229	0.409	0.150
1.580	.292	1.510	.160
3.760	.081	2.460	.051
4.190	.000	2.900	.000

Figure 2.- Wing dimensions. All dimensions are in centimeters.

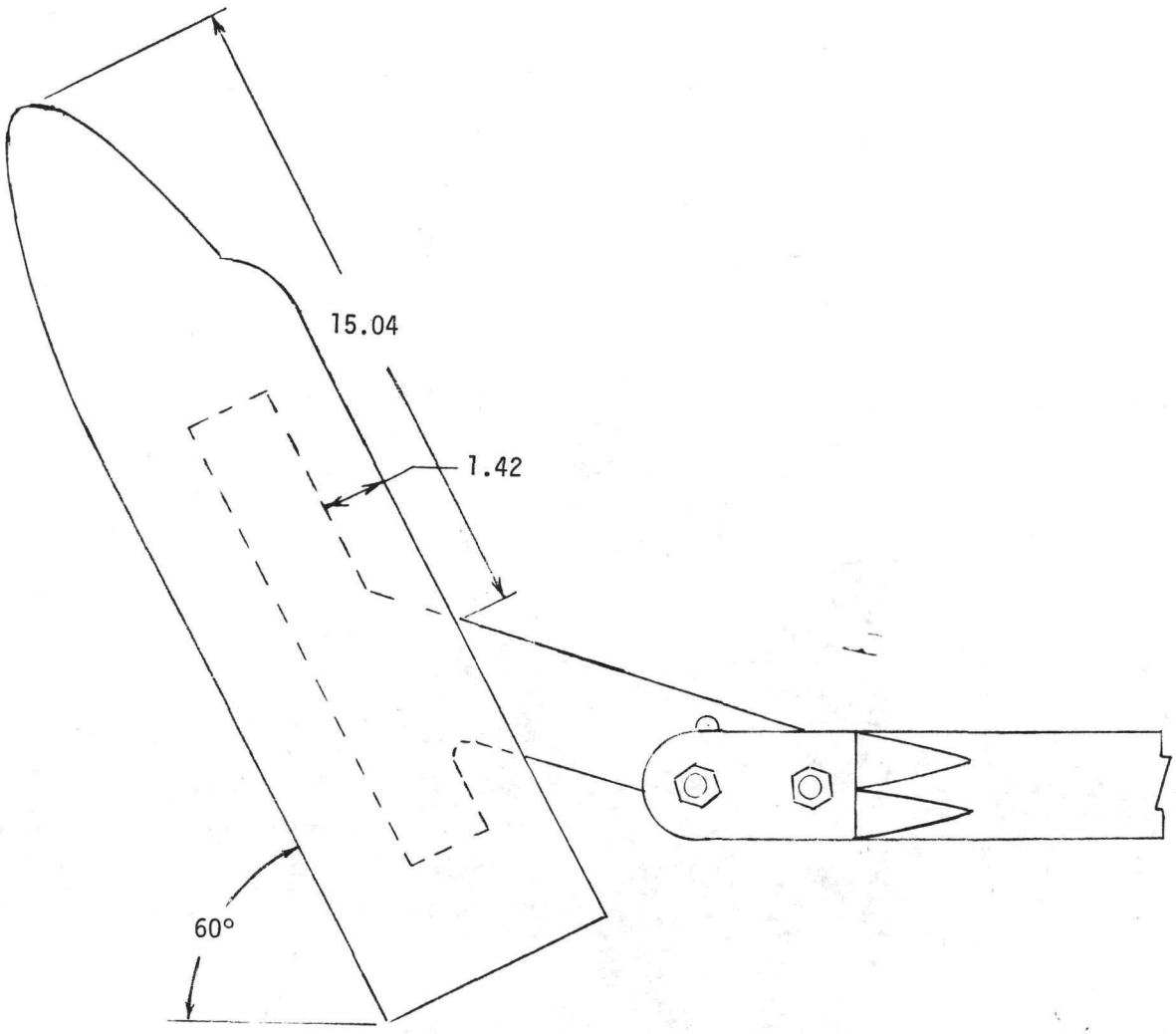

Figure 3.- Model sting. All dimensions are in centimeters.

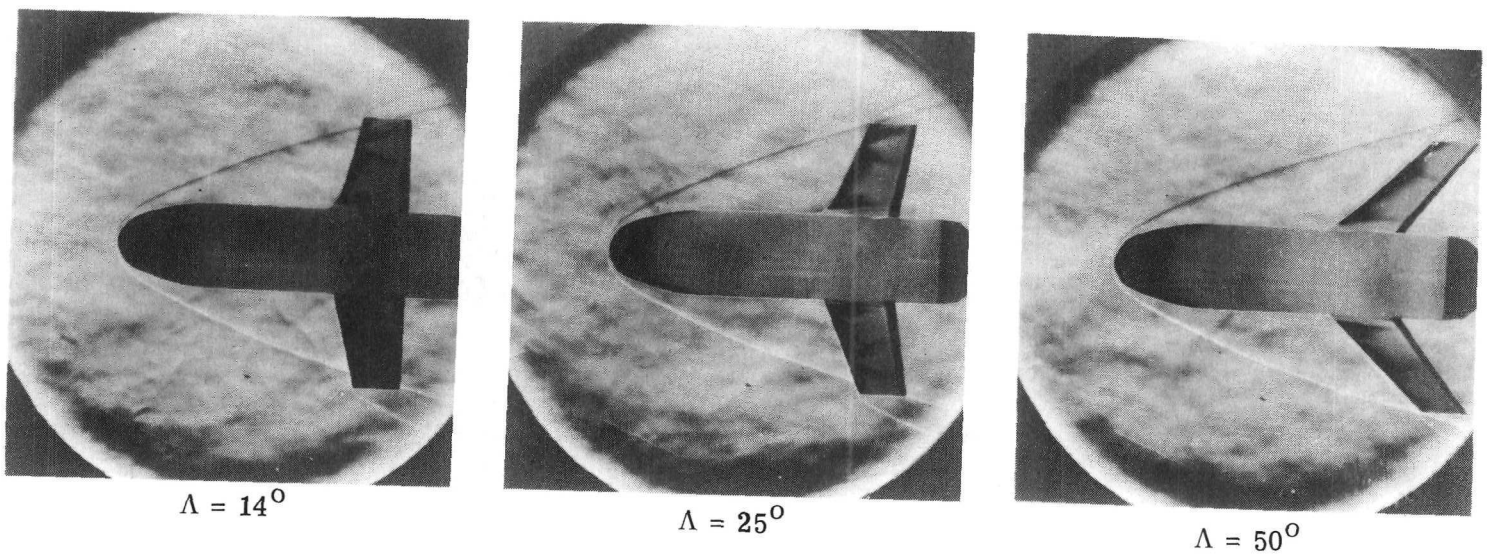

L-72-6583

Figure 4.- Front-lighted schlieren, phase-change patterns. $M_\infty = 7.7$; $\alpha = 30^\circ$; $R_{\infty,l} = 0.47 \times 10^6$.

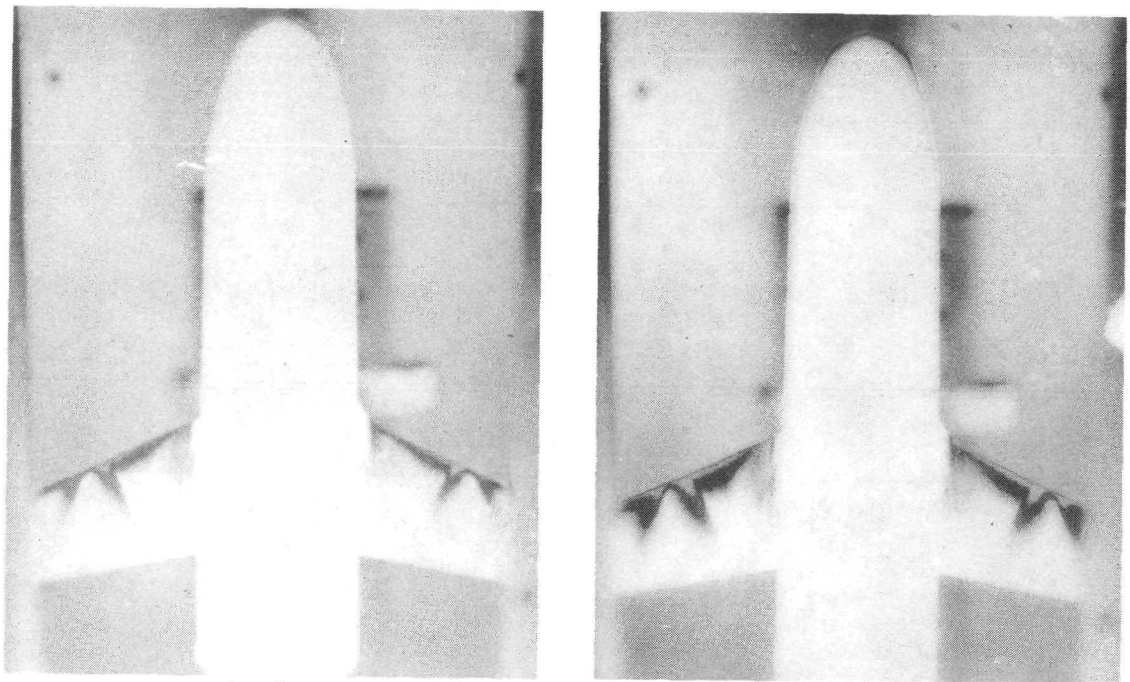

t = 1 sec

t = 2 sec

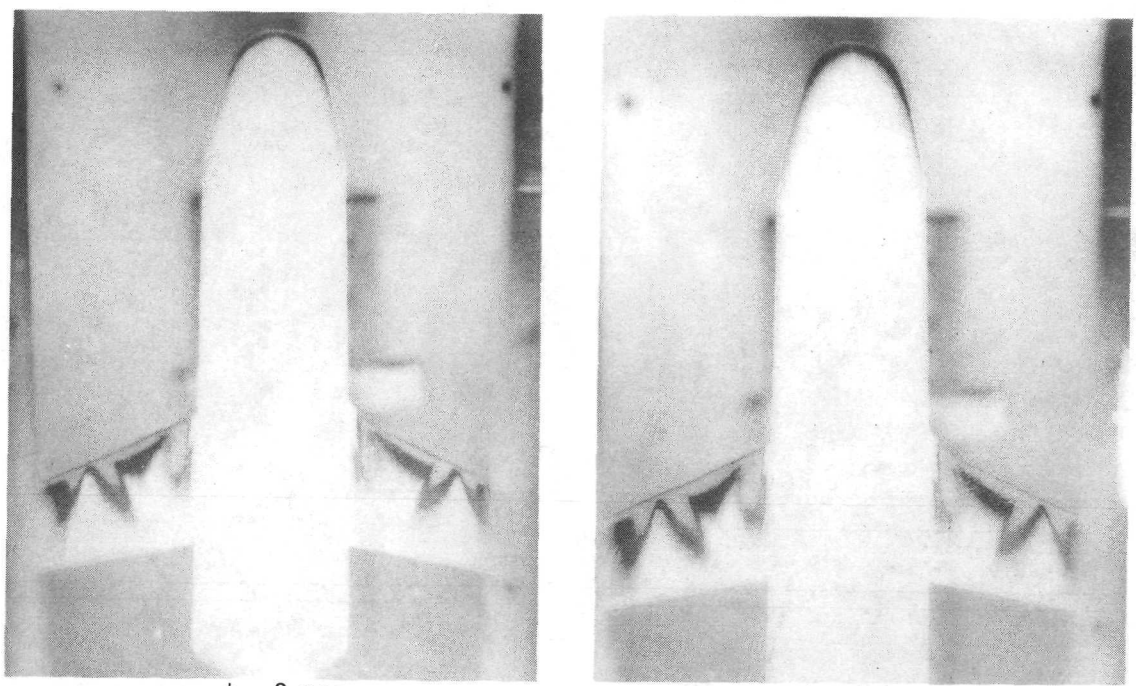

t = 3 sec

t = 4 sec

L-72-6584

Figure 5.- Phase-change patterns for $\Lambda = 25^{o}$, $\alpha = 40^{o}$, and $R_{\infty,l} = 0.47 \times 10^{6}$.

Isotherm	h/h_{ref}
1	0.158
2	.0869
3	.0542
4	.0428
5	.0331
6	.0278

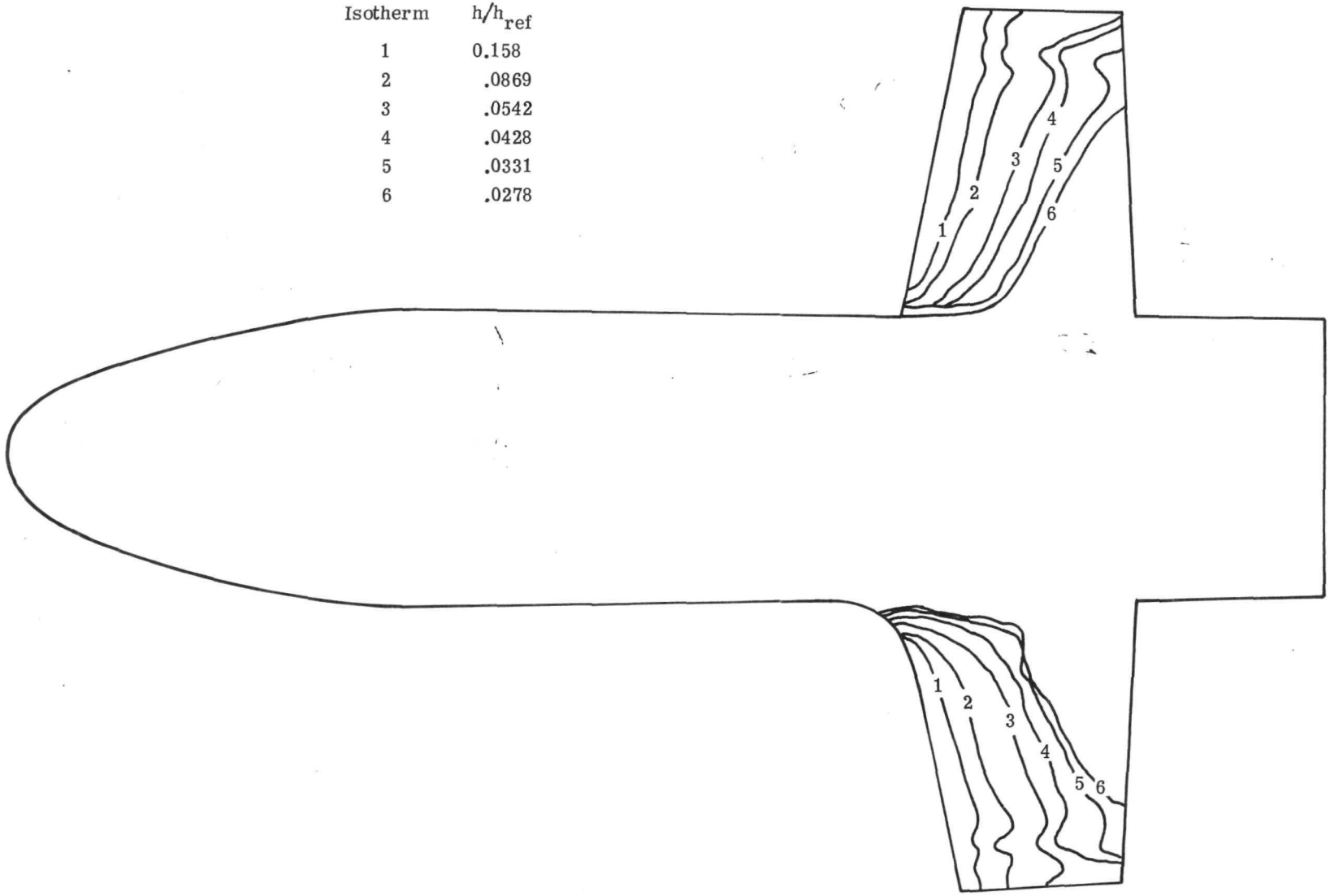

(a) $R_{\infty,\ell} = 0.47 \times 10^6$; $h_{ref} = 619$ W/(m^2-K).

Figure 6.- Heat transfer. $\Lambda = 14^o$; $\alpha = 0^o$.

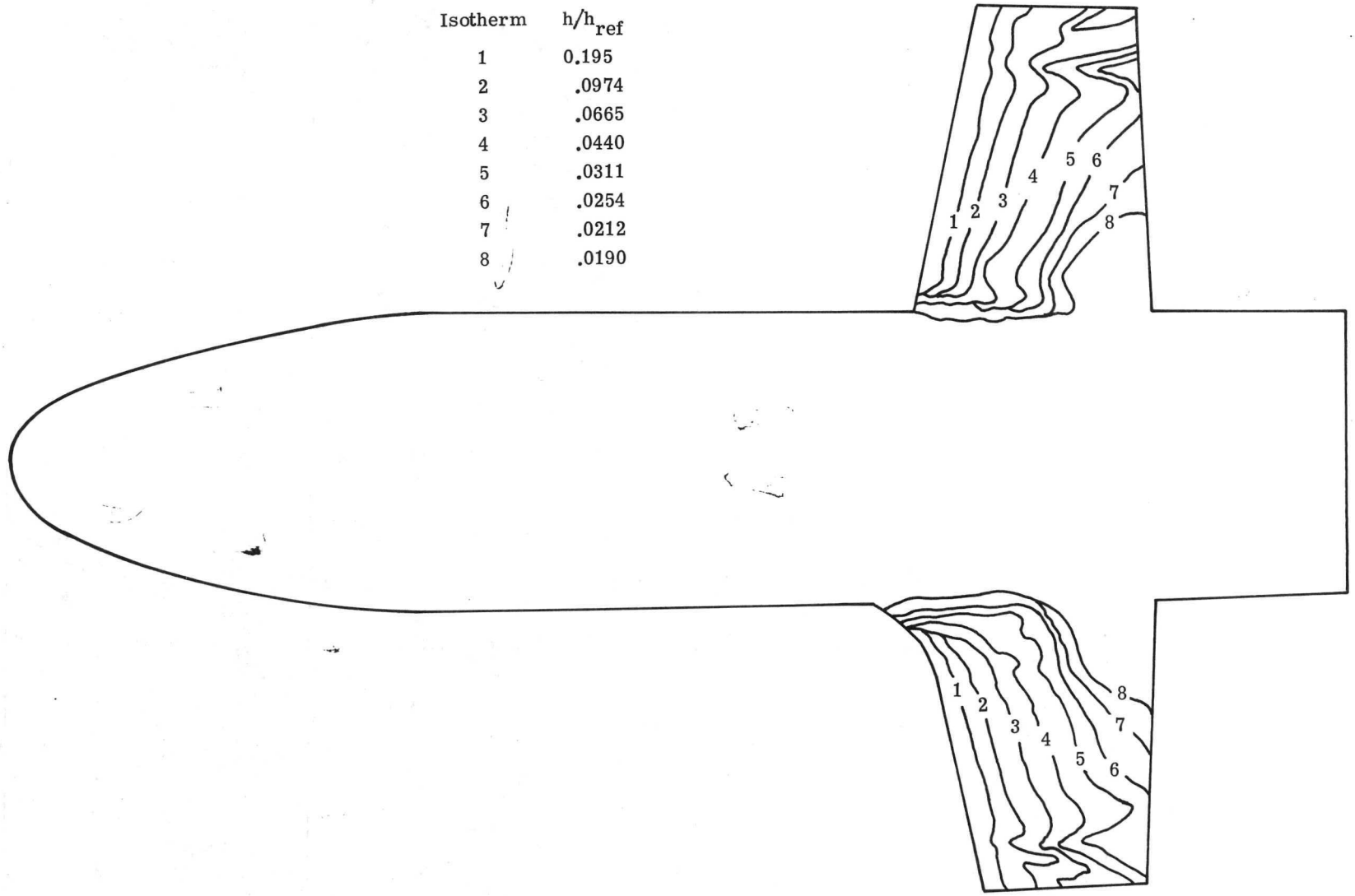

(b) $R_{\infty,l} = 1.7 \times 10^6$; $h_{ref} = 1.23$ kW/(m^2-K).

Figure 6.- Concluded.

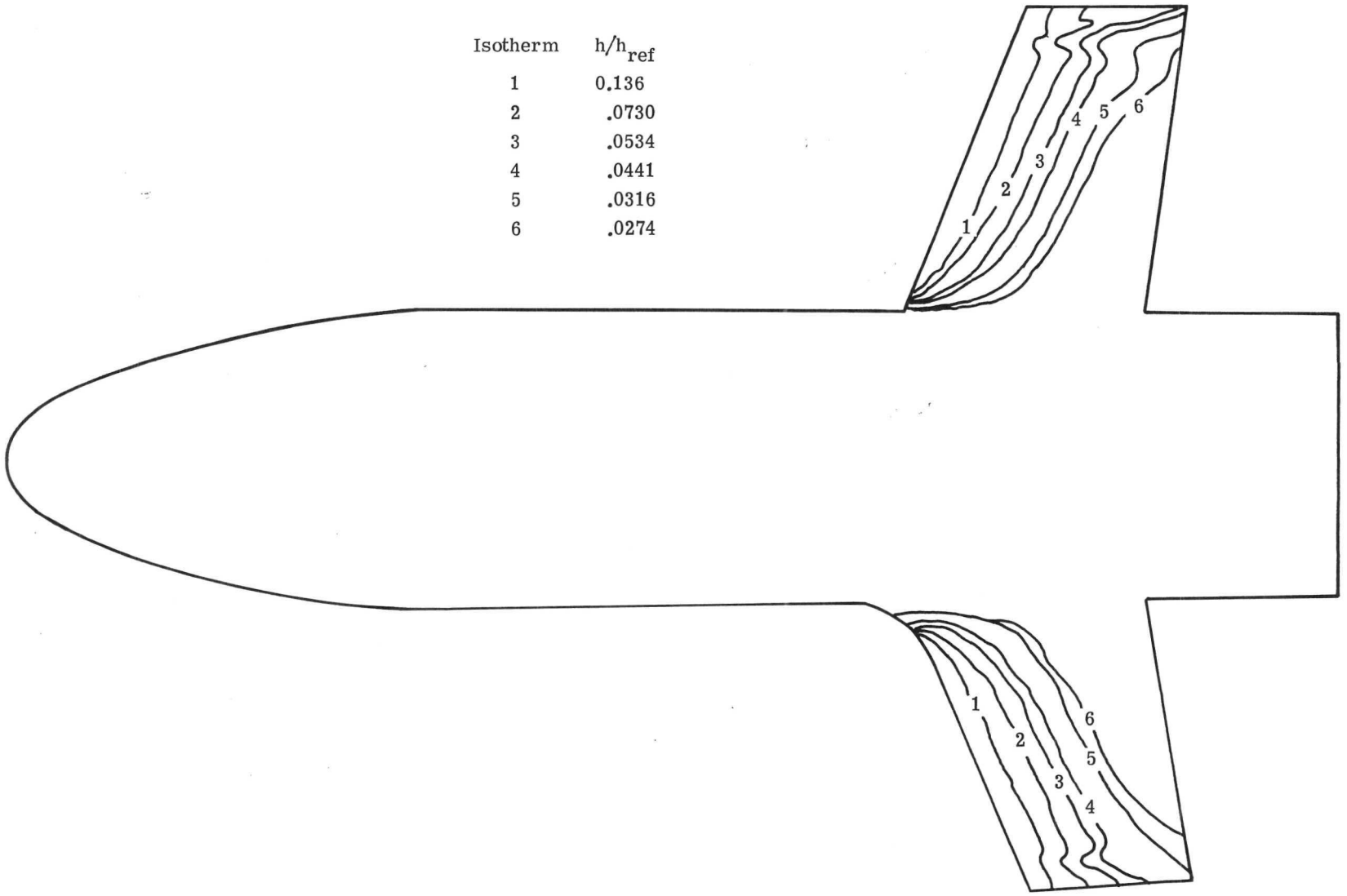

(a) $R_{\infty,l} = 0.47 \times 10^6$; $h_{ref} = 619$ W/(m^2-K).

Figure 7.- Heat transfer. $\Lambda = 25^o$; $\alpha = 0^o$.

Isotherm	h/h_{ref}
1	0.135
2	.0652
3	.0421
4	.0339
5	.0202

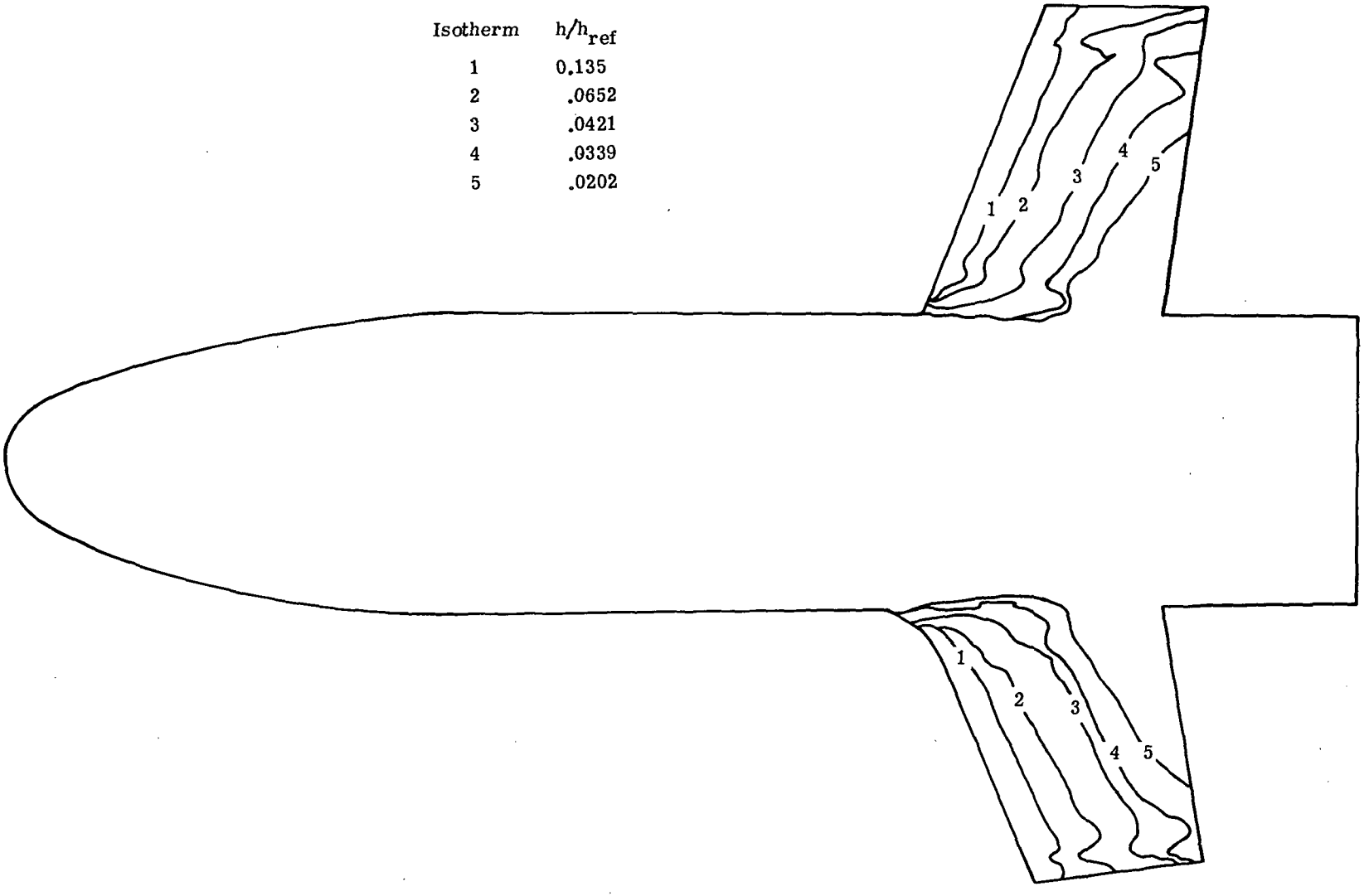

(b) $R_{\infty,l} = 1.7 \times 10^6$; $h_{ref} = 1.23$ kW/(m^2-K).

Figure 7.- Concluded.

Isotherm	h/h_{ref}
1	0.149
2	.0822
3	.0577
4	.0402
5	.0279

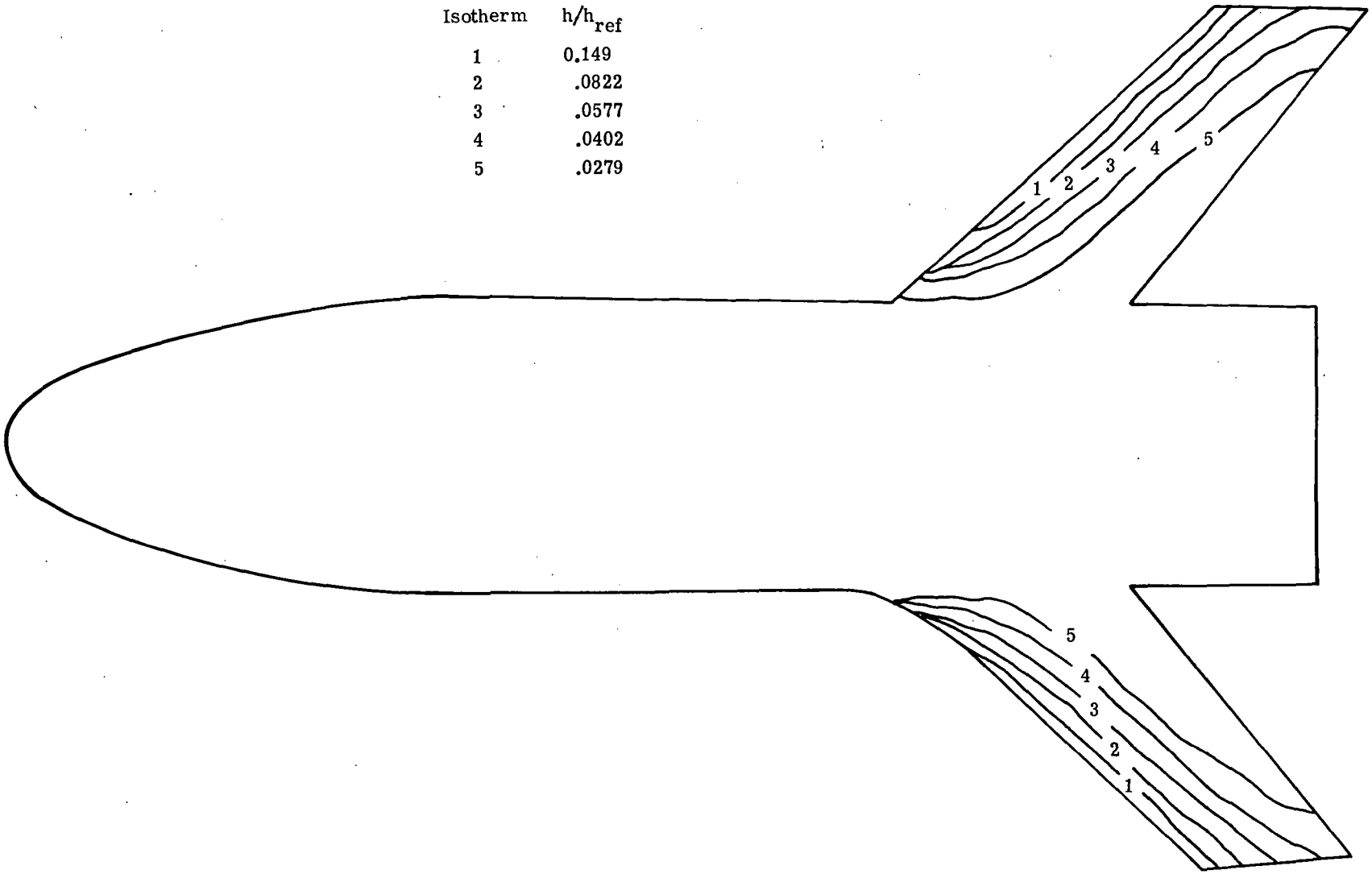

(a) $R_{\infty,l} = 0.47 \times 10^6$; $h_{ref} = 619$ W/(m^2-K).

Figure 8.- Heat transfer. $\Lambda = 50^o$; $\alpha = 0^o$.

Isotherm	h/h_{ref}
1	0.141
2	.0773
3	.0586
4	.0451

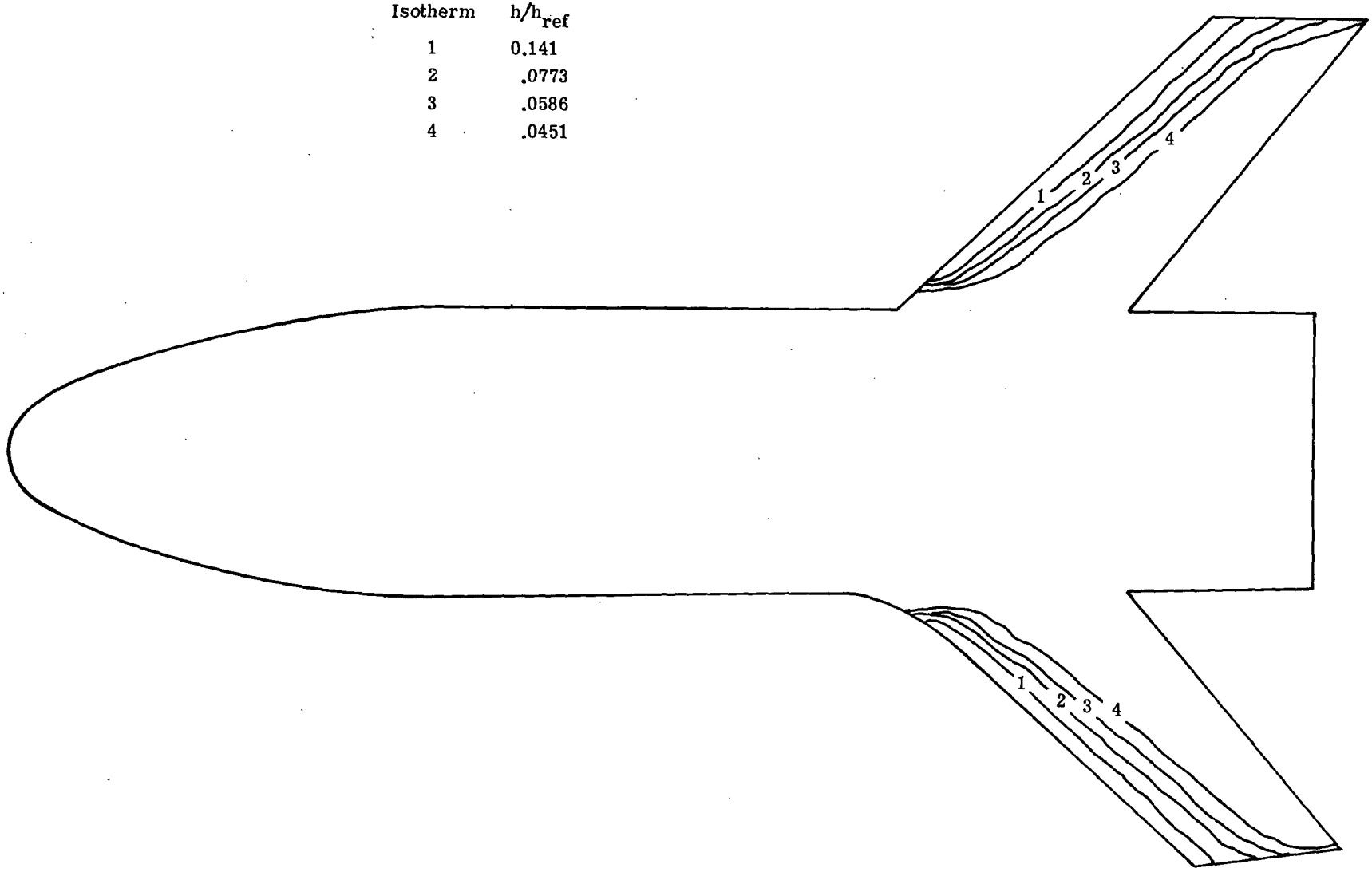

(b) $R_{\infty,\ell} = 1.7 \times 10^6$; $h_{ref} = 1.23$ kW/(m^2-K).

Figure 8.- Concluded.

Isotherm	h/h_{ref}
1	1.109
2	.392
3	.149
4	.103
5	.0809
6	.0648
7	.0544

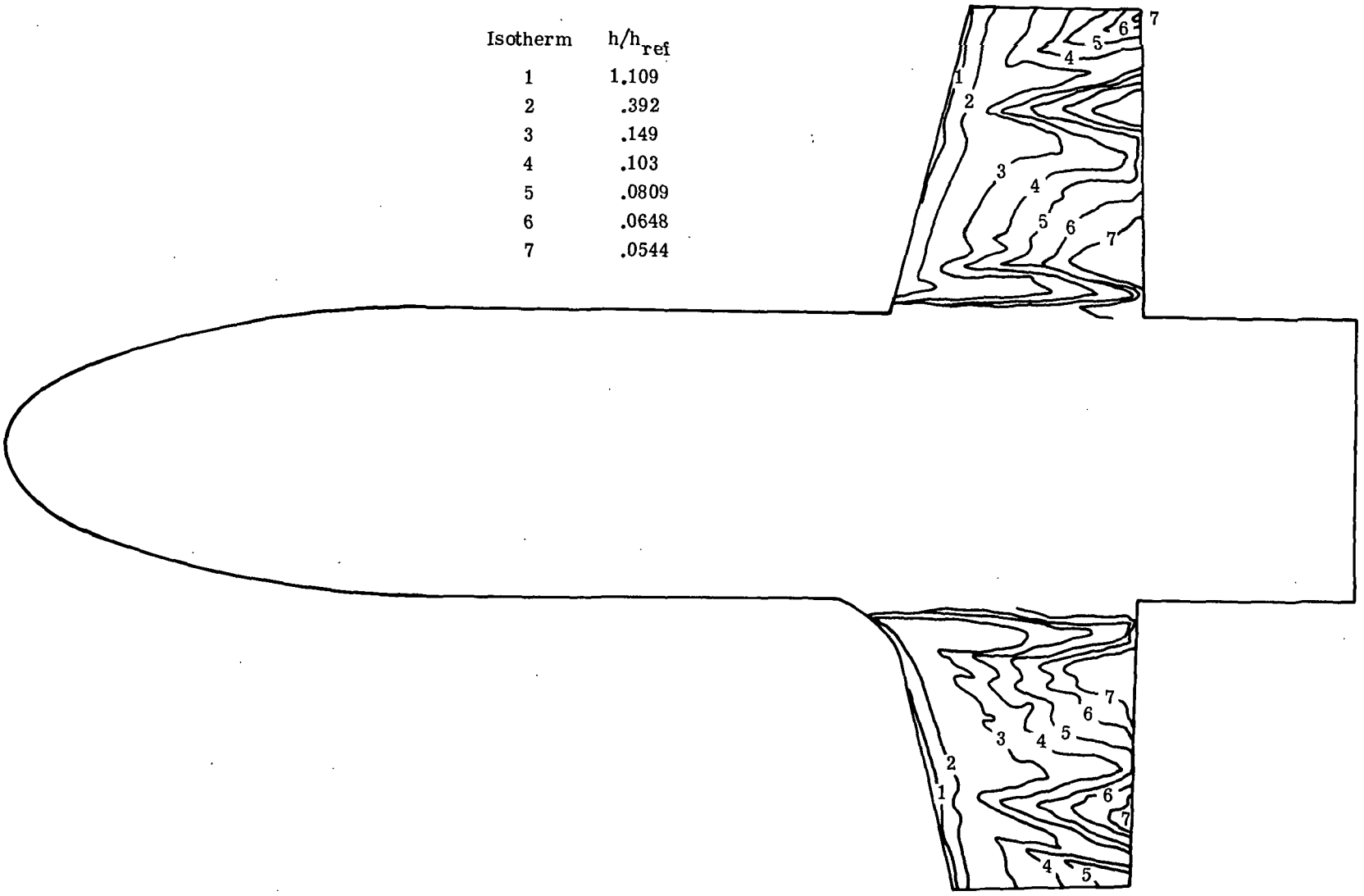

(a) $R_{\infty,\ell} = 0.47 \times 10^6$; $h_{ref} = 619$ W/(m^2-K).

Figure 9.- Heat transfer. $\Lambda = 14^o$; $\alpha = 20^o$.

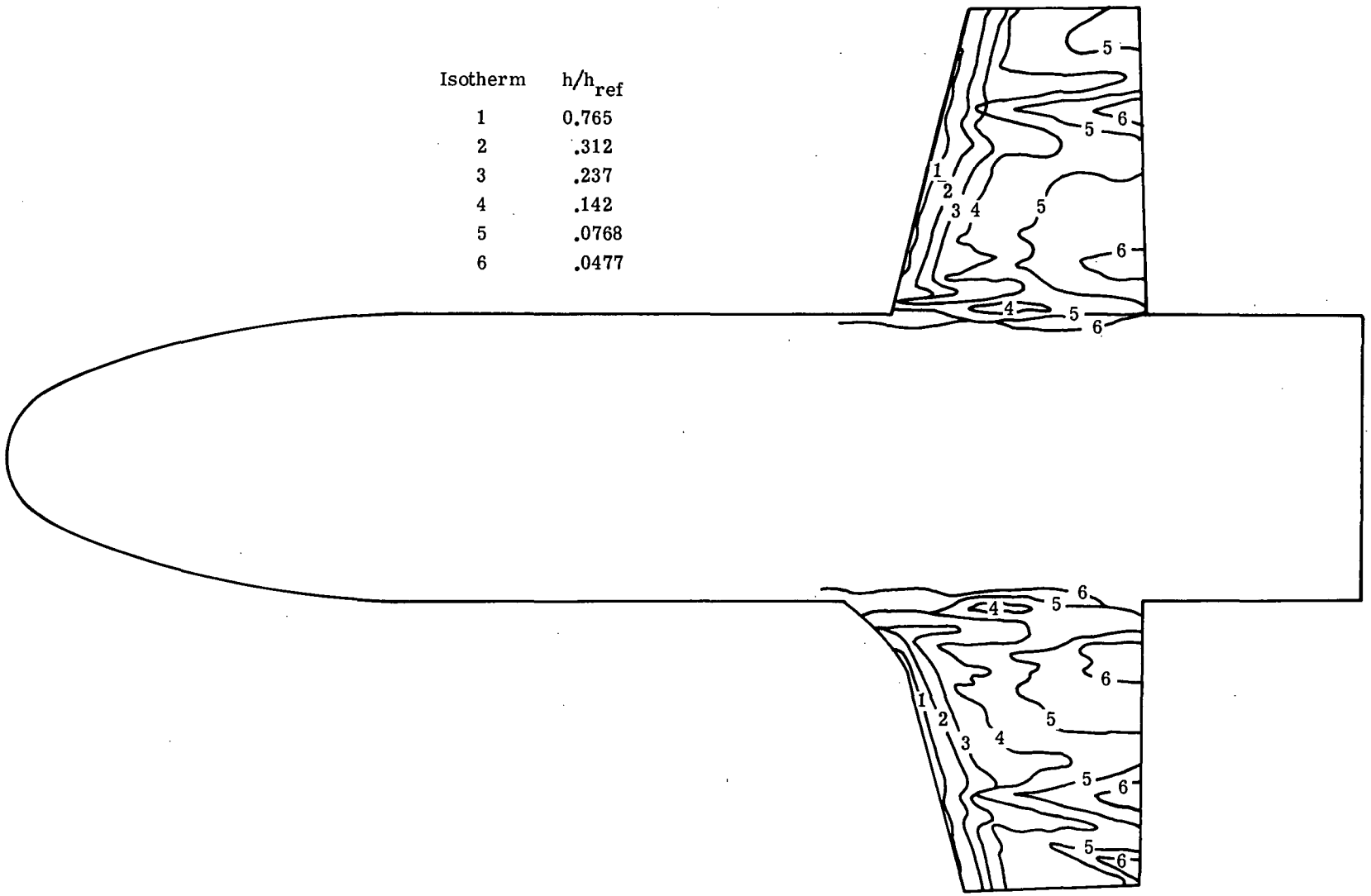

(b) $R_{\infty,l} = 1.7 \times 10^6$; $h_{ref} = 1.23$ kW/(m^2-K).

Figure 9.- Concluded.

Isotherm	h/h_{ref}
1	0.744
2	.372
3	.139
4	.0804
5	.0527
6	.0441

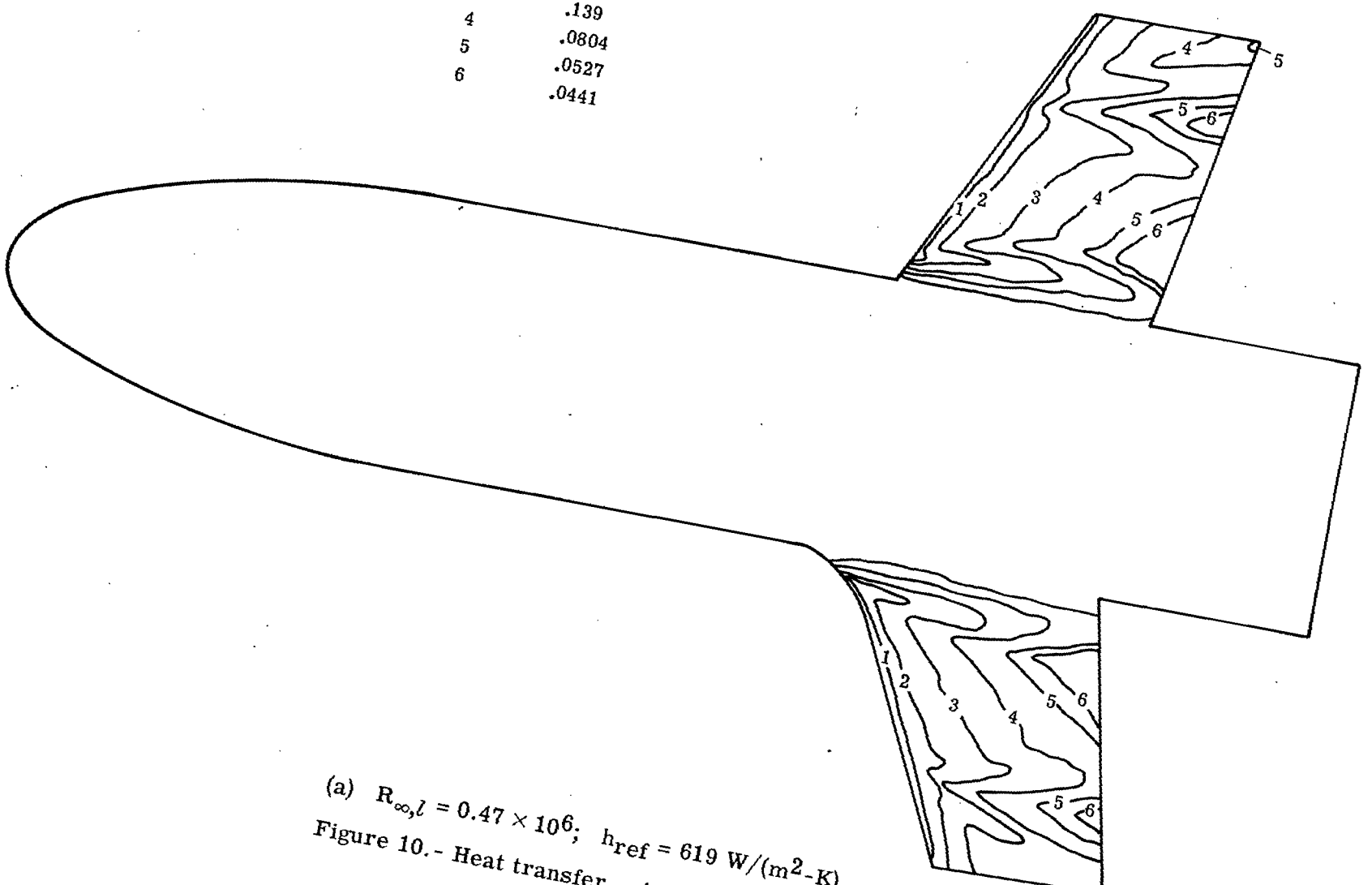

(a) $R_{\infty,l} = 0.47 \times 10^6$; $h_{ref} = 619$ W/(m^2-K).

Figure 10.- Heat transfer. $\Lambda = 25^o$; $\alpha = 20^o$.

Isotherm	h/h_{ref}
1	0.553
2	.226
3	.132
4	.0764
5	.0592

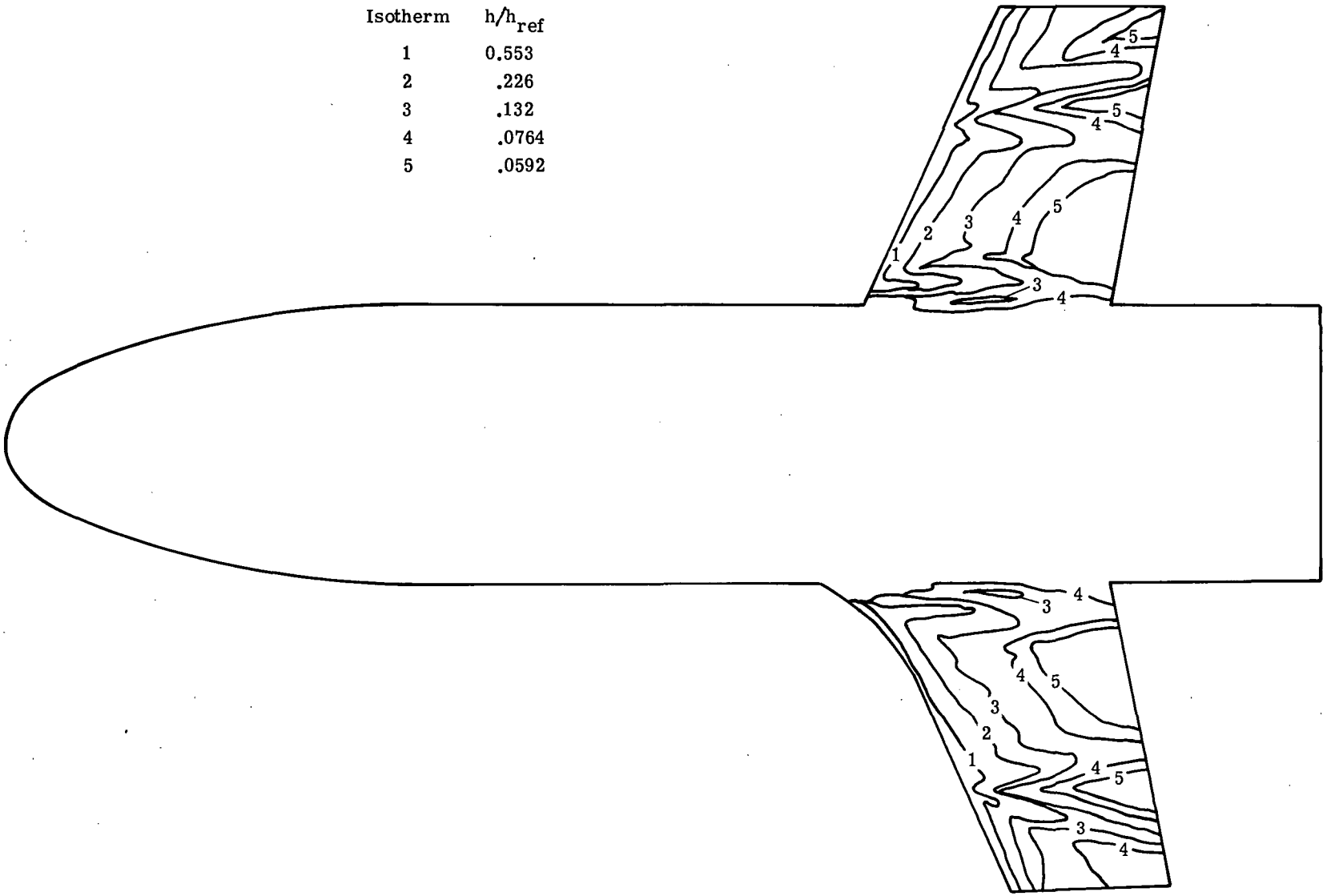

(b) $R_{\infty,l} = 1.7 \times 10^6$; $h_{ref} = 1.23$ kW/(m^2-K).

Figure 10.- Concluded.

Isotherm	h/h_{ref}
1	0.811
2	.363
3	.244
4	.0844
5	.0654
6	.0553
7	.0462

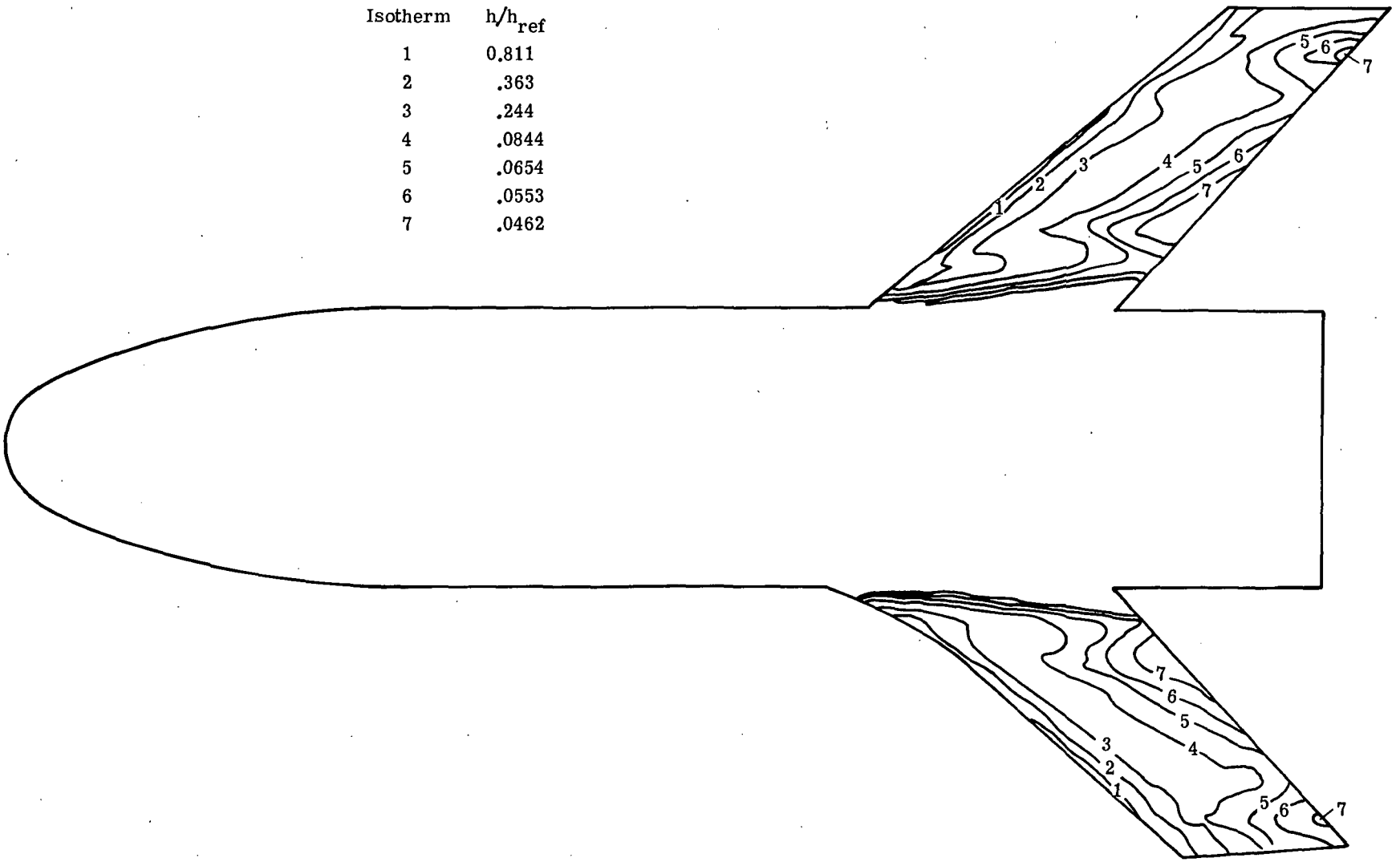

(a) $R_{\infty,l} = 0.47 \times 10^6$; $h_{ref} = 619$ W/(m^2-K).

Figure 11.- Heat transfer. $\Lambda = 50^o$; $\alpha = 20^o$.

Isotherm	h/h_{ref}
1	0.581
2	.252
3	.140
4	.0990
5	.0572

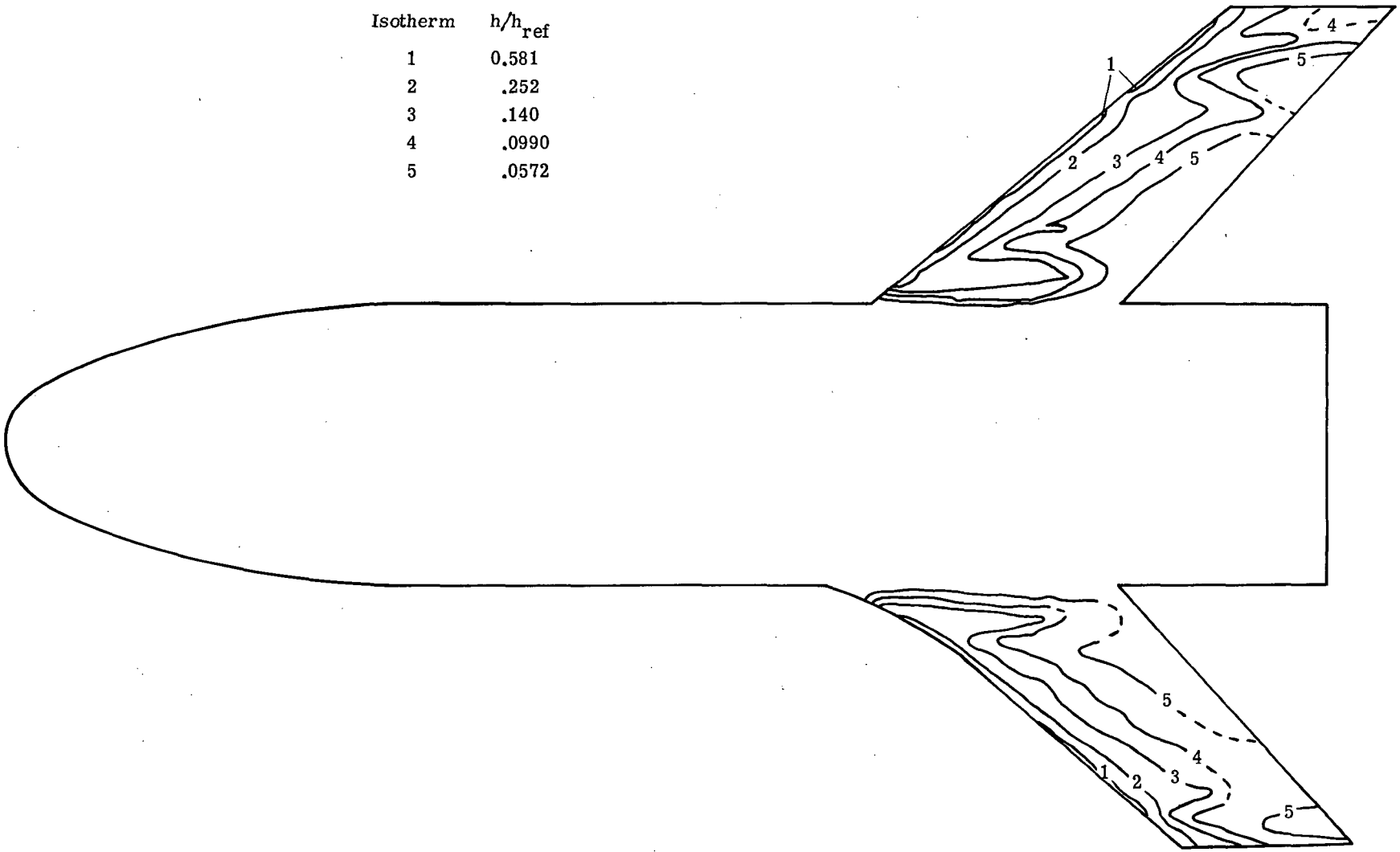

(b) $R_{\infty,l} = 1.7 \times 10^6$; $h_{ref} = 1.23$ kW/(m^2-K).

Figure 11.- Concluded.

Isotherm	h/h_{ref}
1	1.454
2	.514
3	.320
4	.185
5	.143
6	.0965
7	.0835

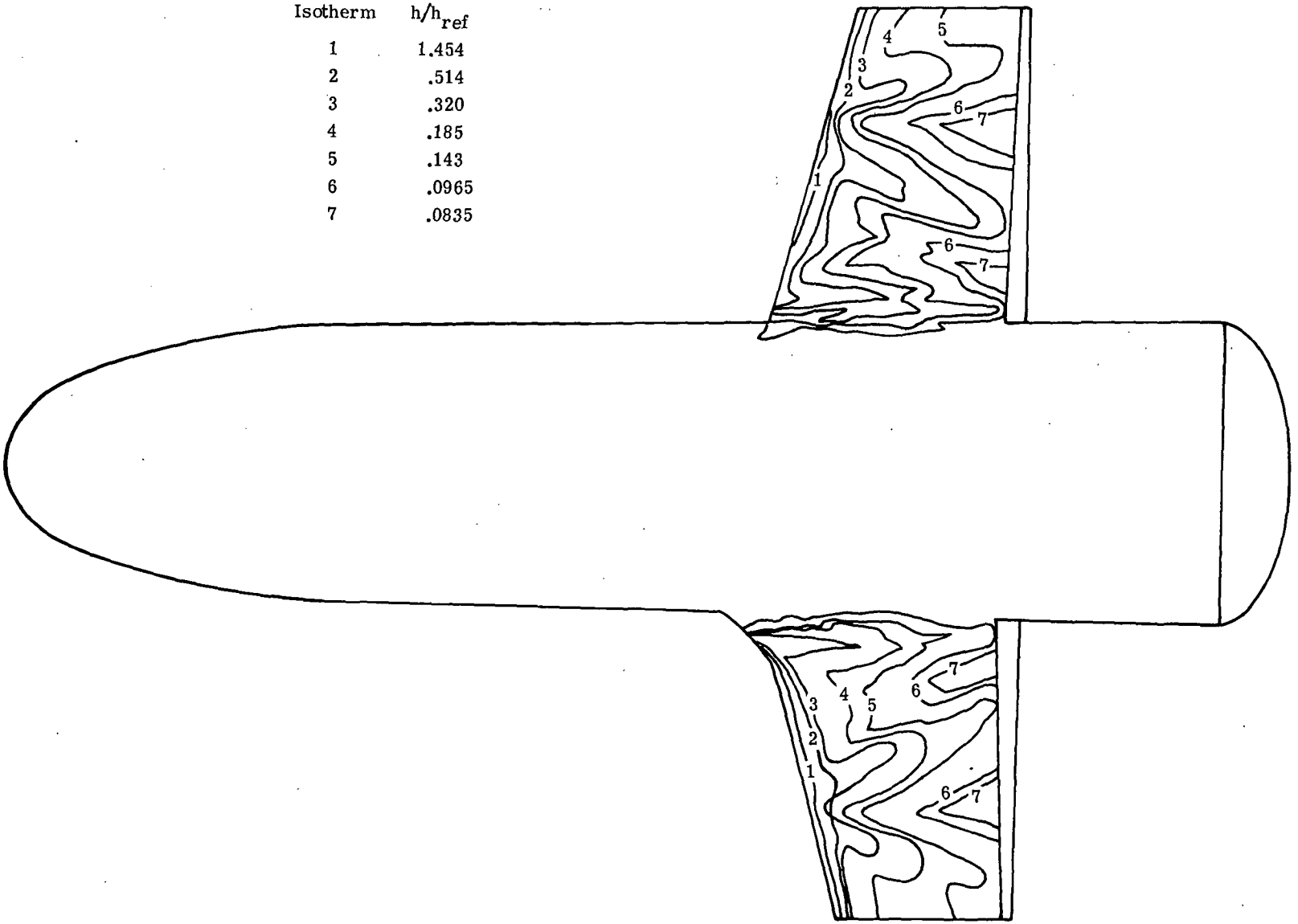

(a) $R_{\infty,l} = 0.47 \times 10^6$; $h_{ref} = 619$ W/(m^2-K).

Figure 12.- Heat transfer. $\Lambda = 14^o$; $\alpha = 40^o$.

Isotherm	h/h_{ref}
1	1.154
2	.516
3	.365
4	.320
5	.227
6	.130

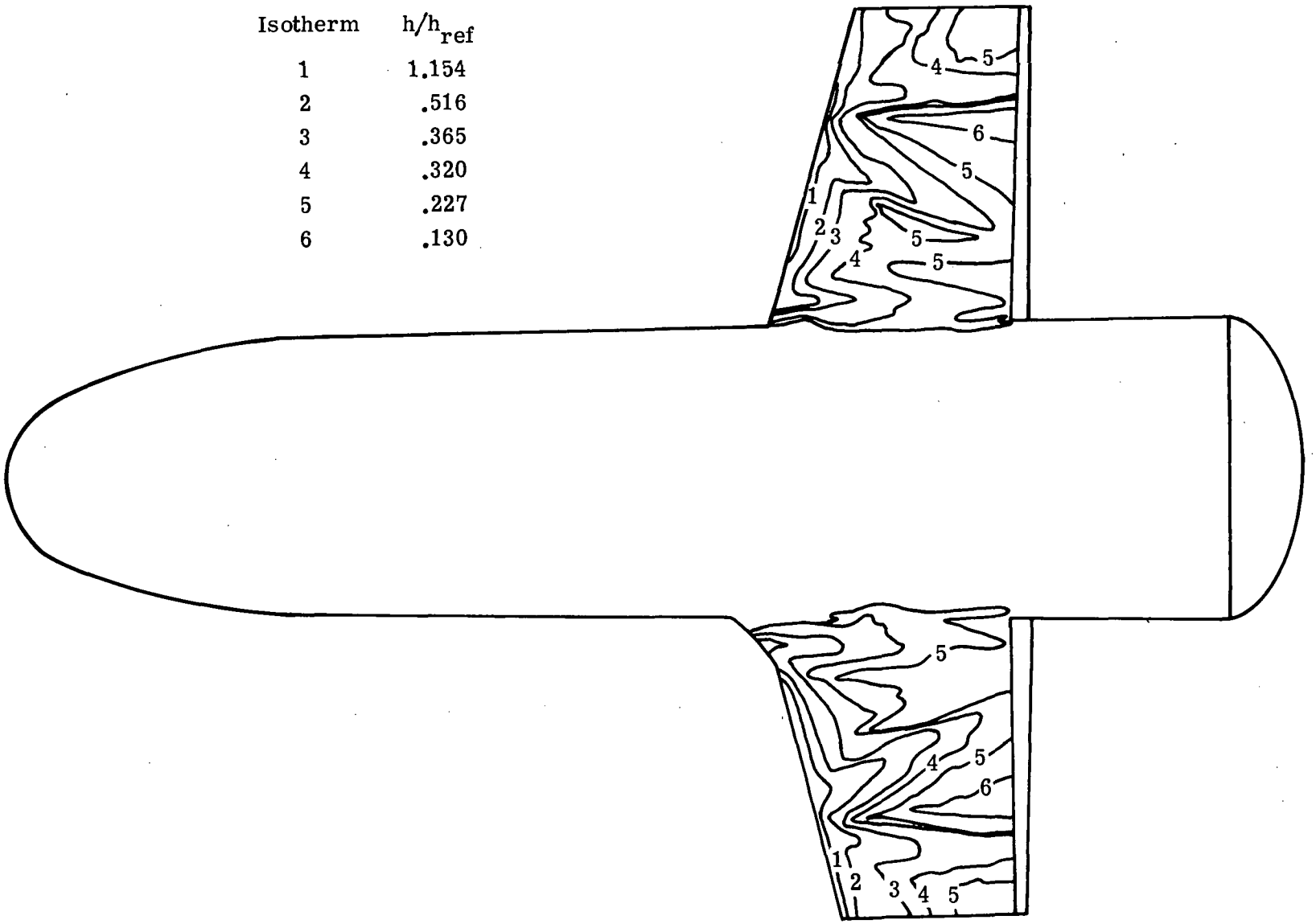

(b) $R_{\infty,\ell} = 1.7 \times 10^6$; $h_{ref} = 1.23$ kW/(m^2-K).

Figure 12.- Concluded.

Isotherm	h/h_{ref}
1	1.446
2	.590
3	.342
4	.197
5	.153
6	.114
7	.0883

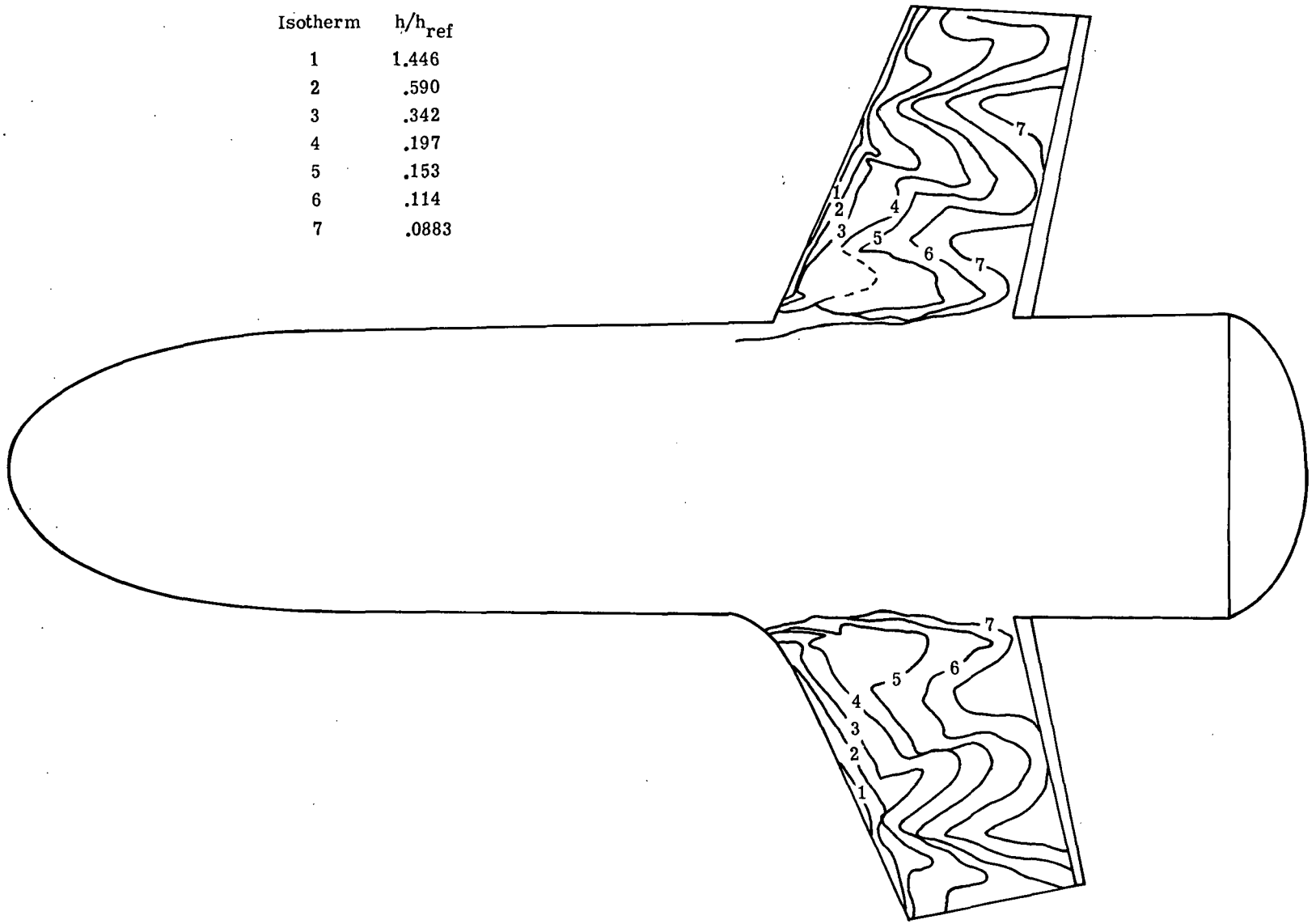

(a) $R_{\infty,l} = 0.47 \times 10^6$; $h_{ref} = 619$ W/(m^2-K).

Figure 13.- Heat transfer. $\Lambda = 25^o$; $\alpha = 40^o$.

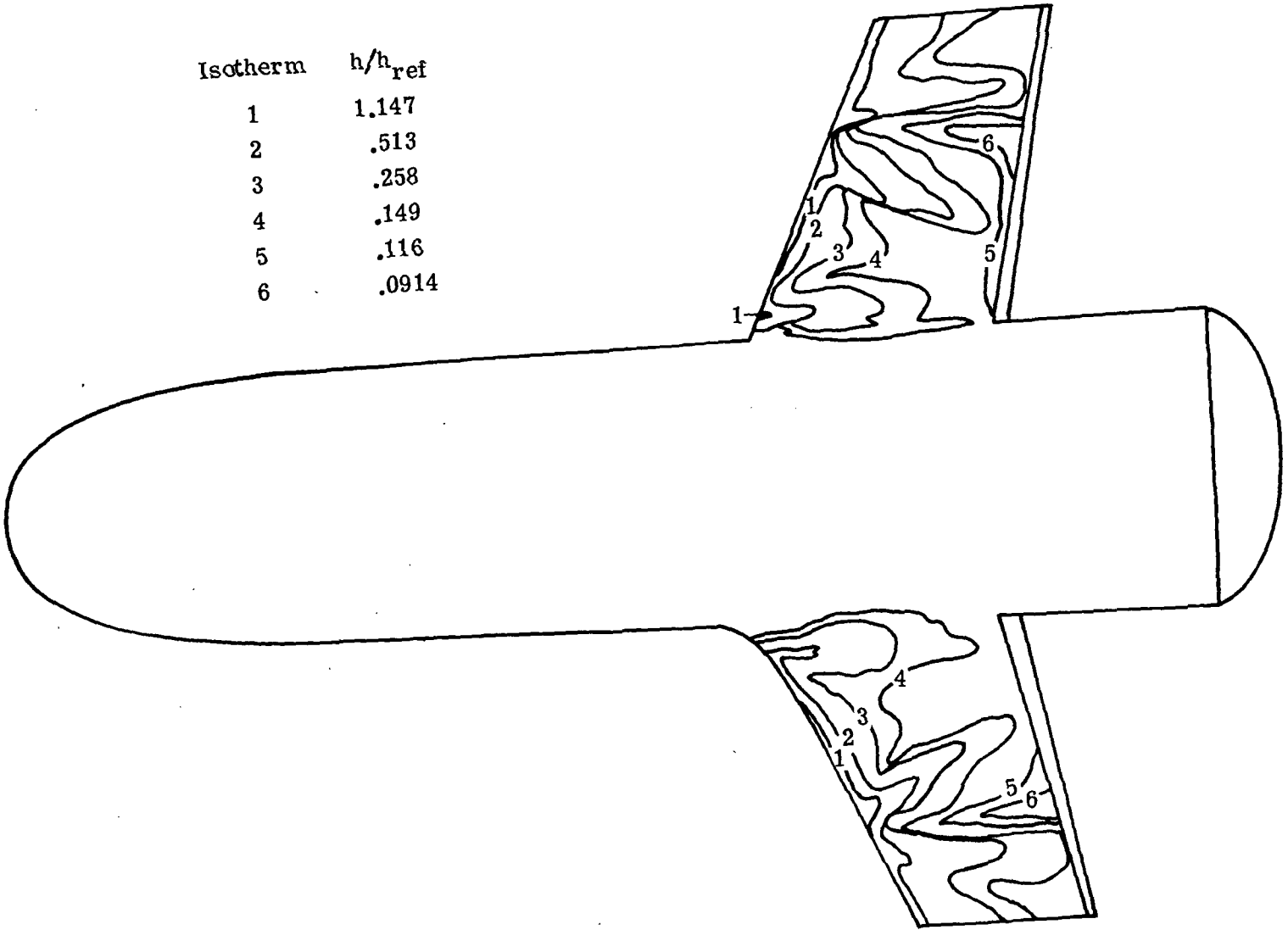

(b) $R_{\infty,l} = 1.7 \times 10^6$; $h_{ref} = 1.23$ kW/(m^2-K).

Figure 13.- Concluded.

Isotherm	h/h_{ref}
1	0.351
2	.248
3	.203
4	.157
5	.117
6	.0975

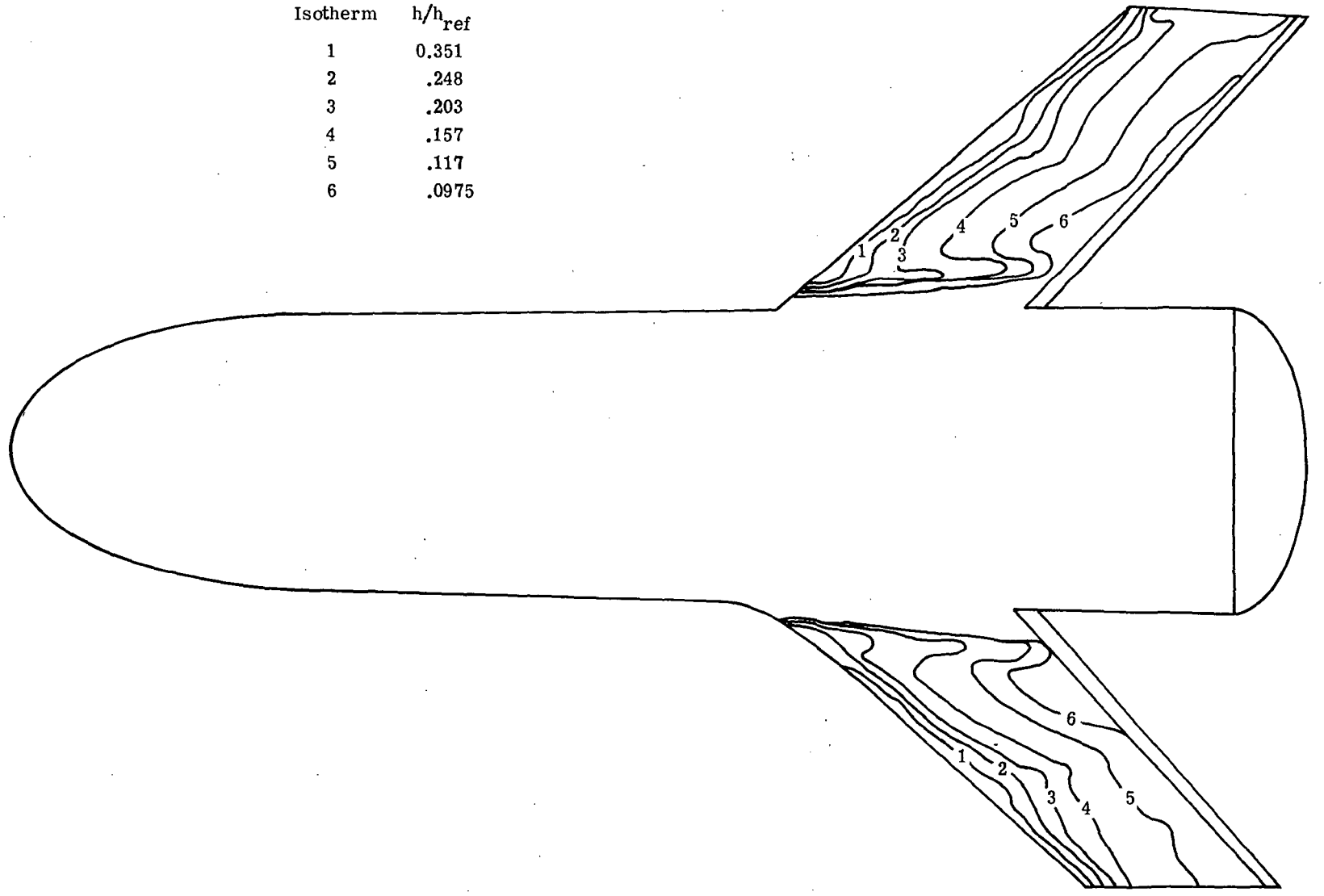

(a) $R_{\infty,l} = 0.47 \times 10^6$; $h_{ref} = 619$ W/(m^2-K).

Figure 14.- Heat transfer. $\Lambda = 50^o$; $\alpha = 40^o$.

Isotherm	h/h_{ref}
1	0.777
2	.449
3	.294
4	.271
5	.221
6	.192
7	.168
8	.135

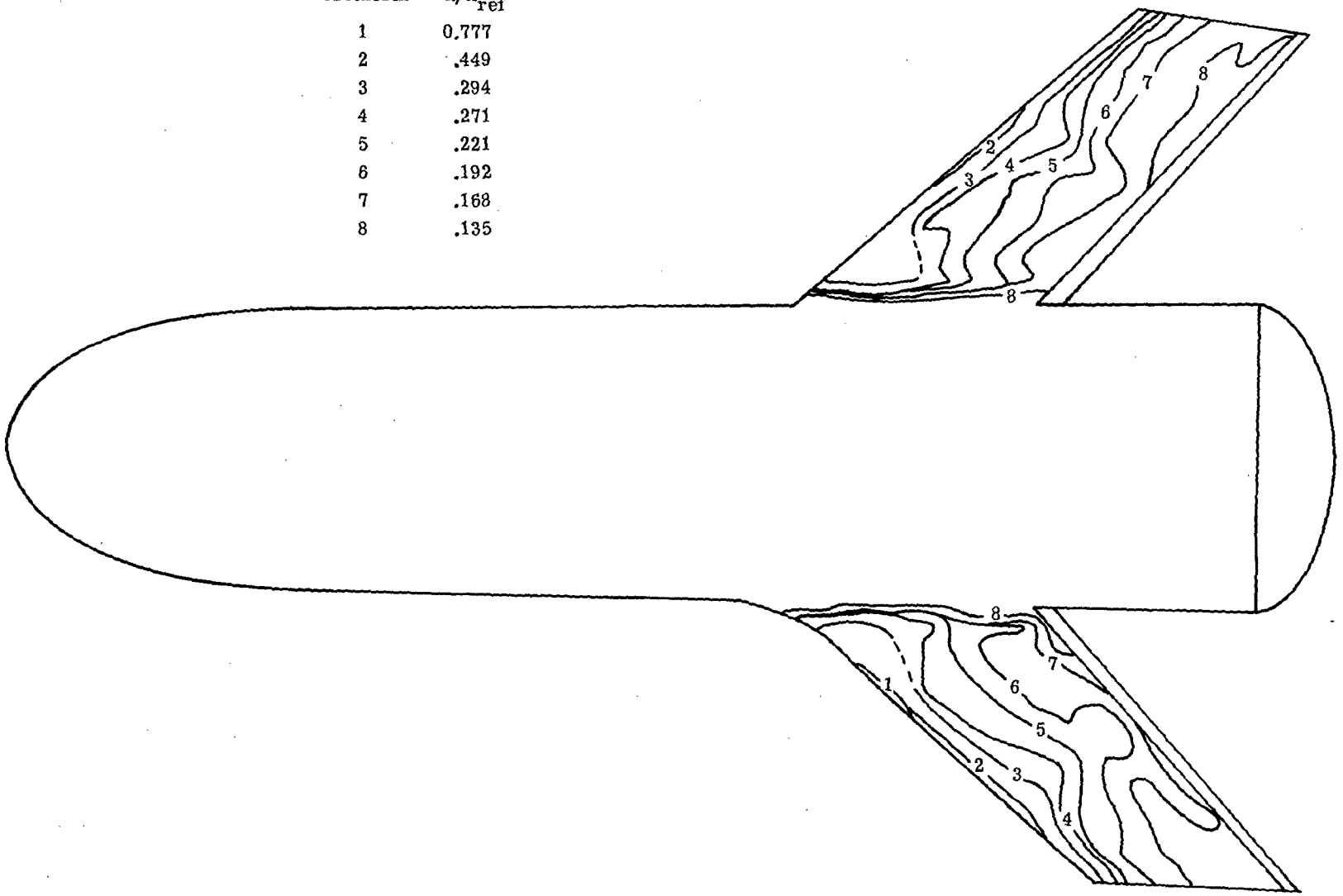

(b) $R_{\infty,l} = 1.7 \times 10^6$; $h_{ref} = 1.23$ kW/(m^2-K).

Figure 14.- Concluded.

Isotherm	h/h_{ref}
1	0.447
2	.316
3	.223
4	.184
5	.158
6	.141
7	.132

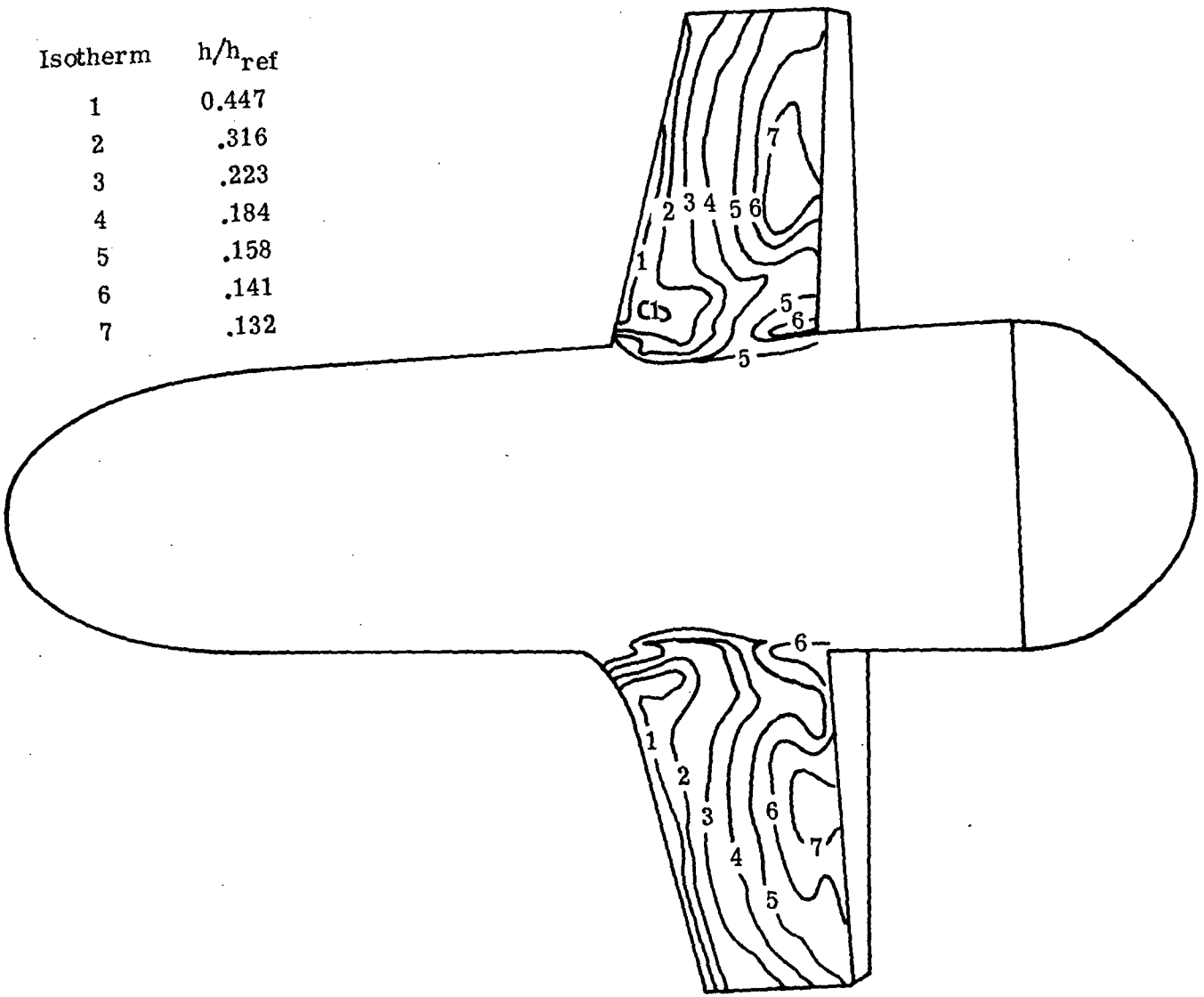

(a) $R_{\infty,l} = 0.47 \times 10^6$; $h_{ref} = 619\ W/(m^2\text{-}K)$.

Figure 15.- Heat transfer. $\Lambda = 14^o$; $\alpha = 60^o$.

Isotherm	h/h_{ref}
1	0.870
2	.688
3	.486
4	.373
5	.263
6	.215
7	.186
8	.152

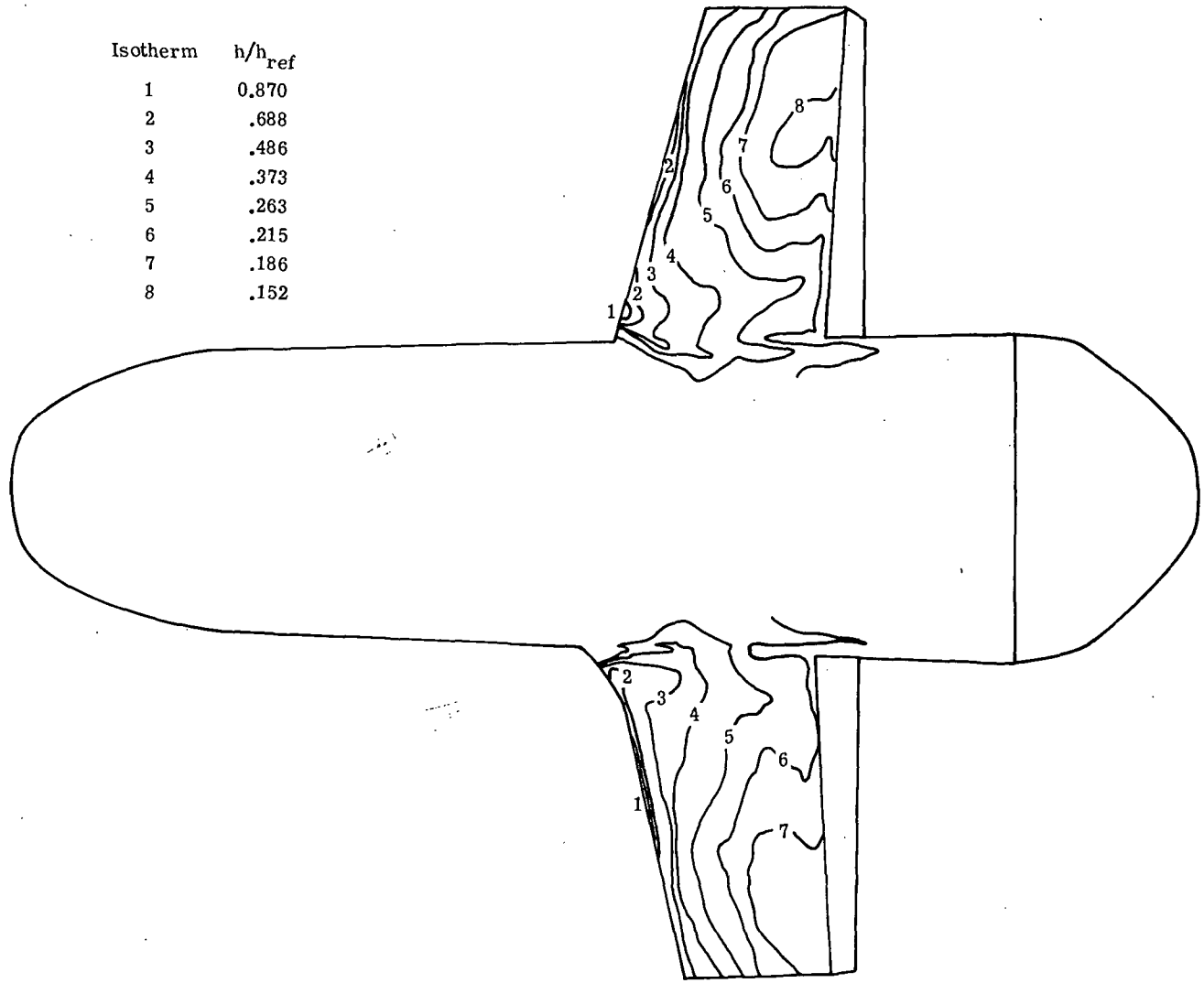

(b) $R_{\infty,l} = 1.7 \times 10^6$; $h_{ref} = 1.23$ kW/(m^2-K).

Figure 15.- Concluded.

Isotherm	h/h_{ref}
1	0.443
2	.314
3	.256
4	.198
5	.157
6	.140
7	.128

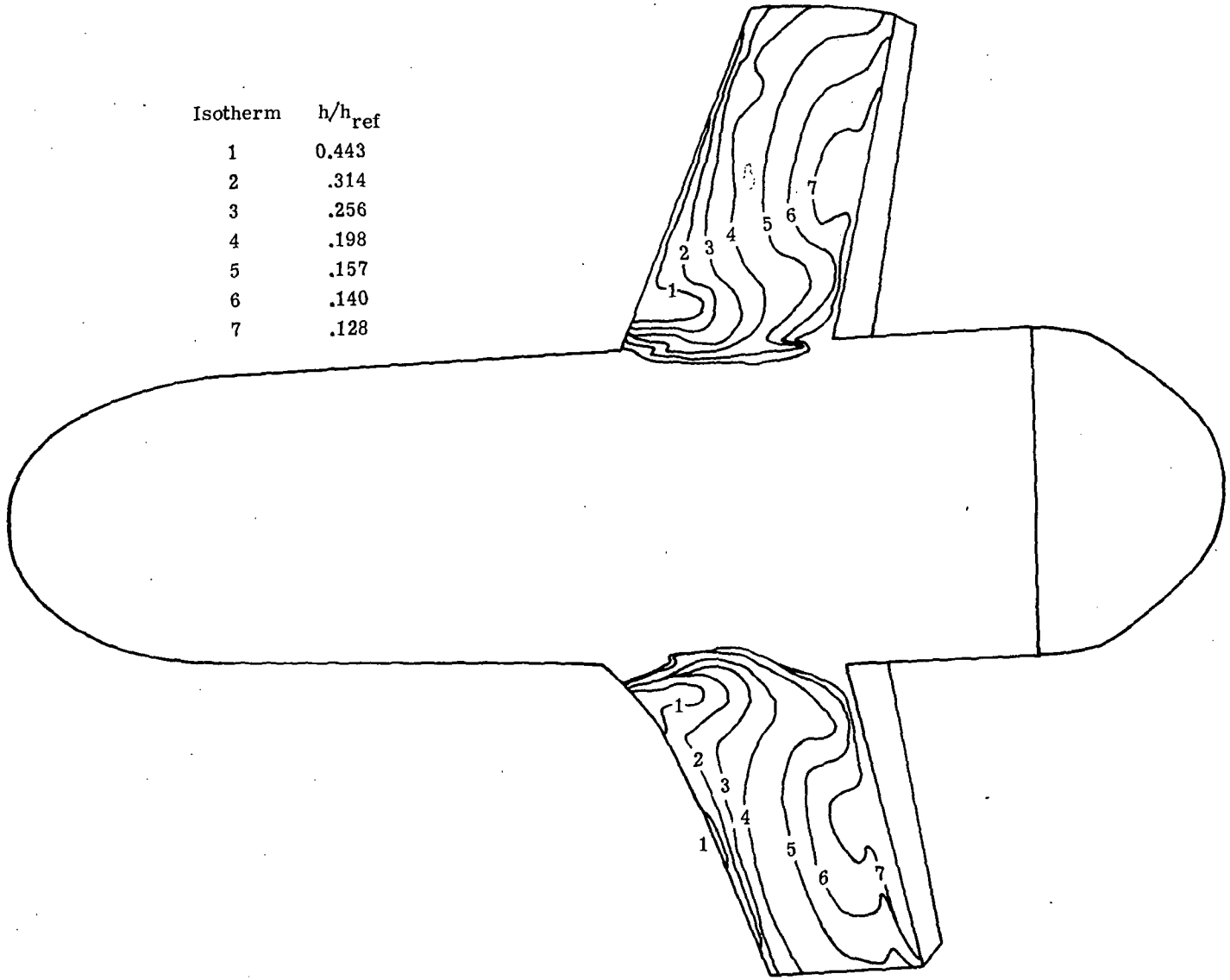

(a) $R_{\infty,l} = 0.47 \times 10^6$; $h_{ref} = 619$ W/(m^2-K).

Figure 16.- Heat-transfer. $\Lambda = 25^o$; $\alpha = 60^o$.

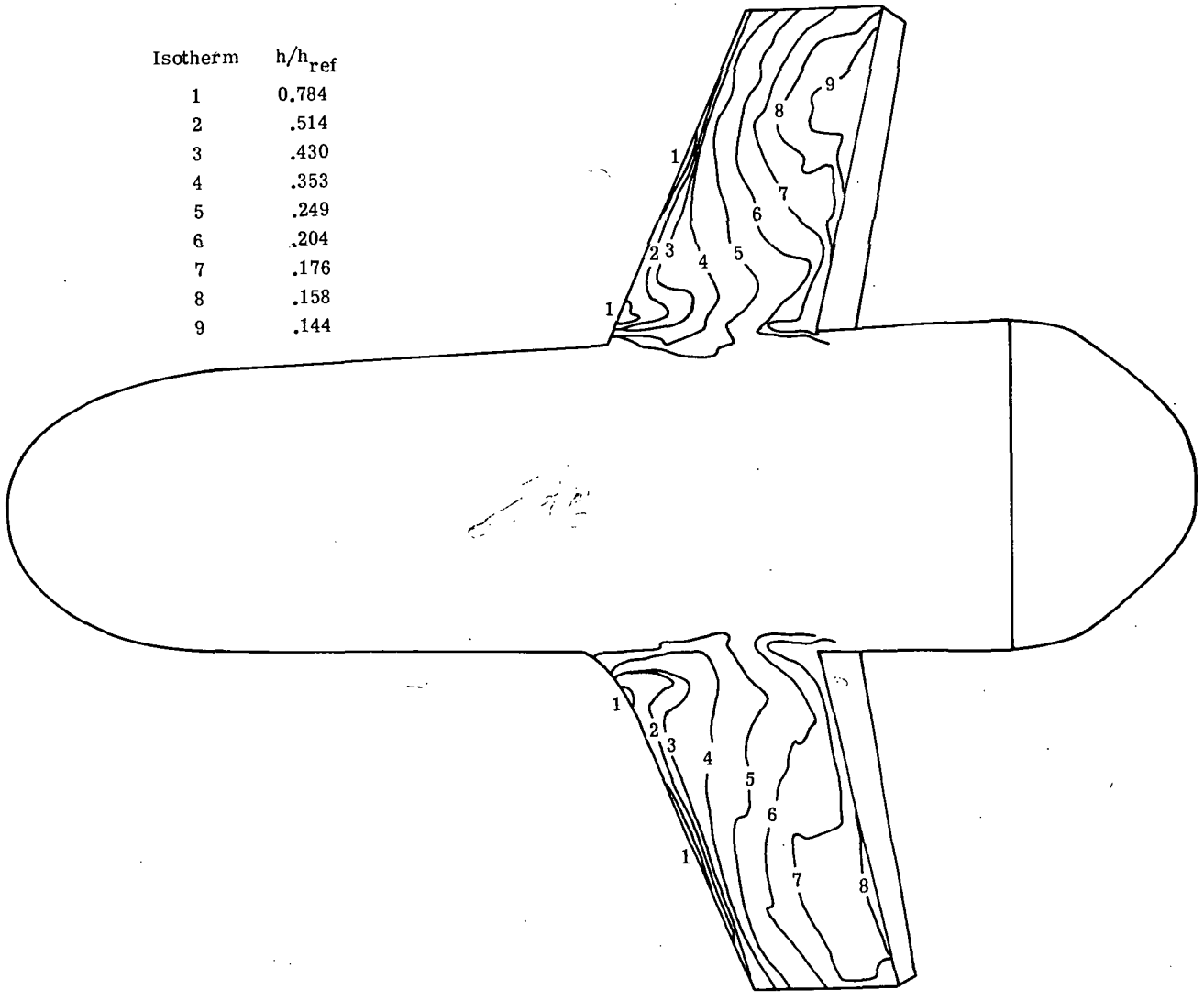

(b) $R_{\infty,l} = 1.7 \times 10^6$; $h_{ref} = 1.23$ kW/(m^2-K).

Figure 16.- Concluded.

Isotherm	h/h_{ref}
1	0.265
2	.229
3	.205
4	.187
5	.162
6	.153
7	.145
8	.132
9	.116

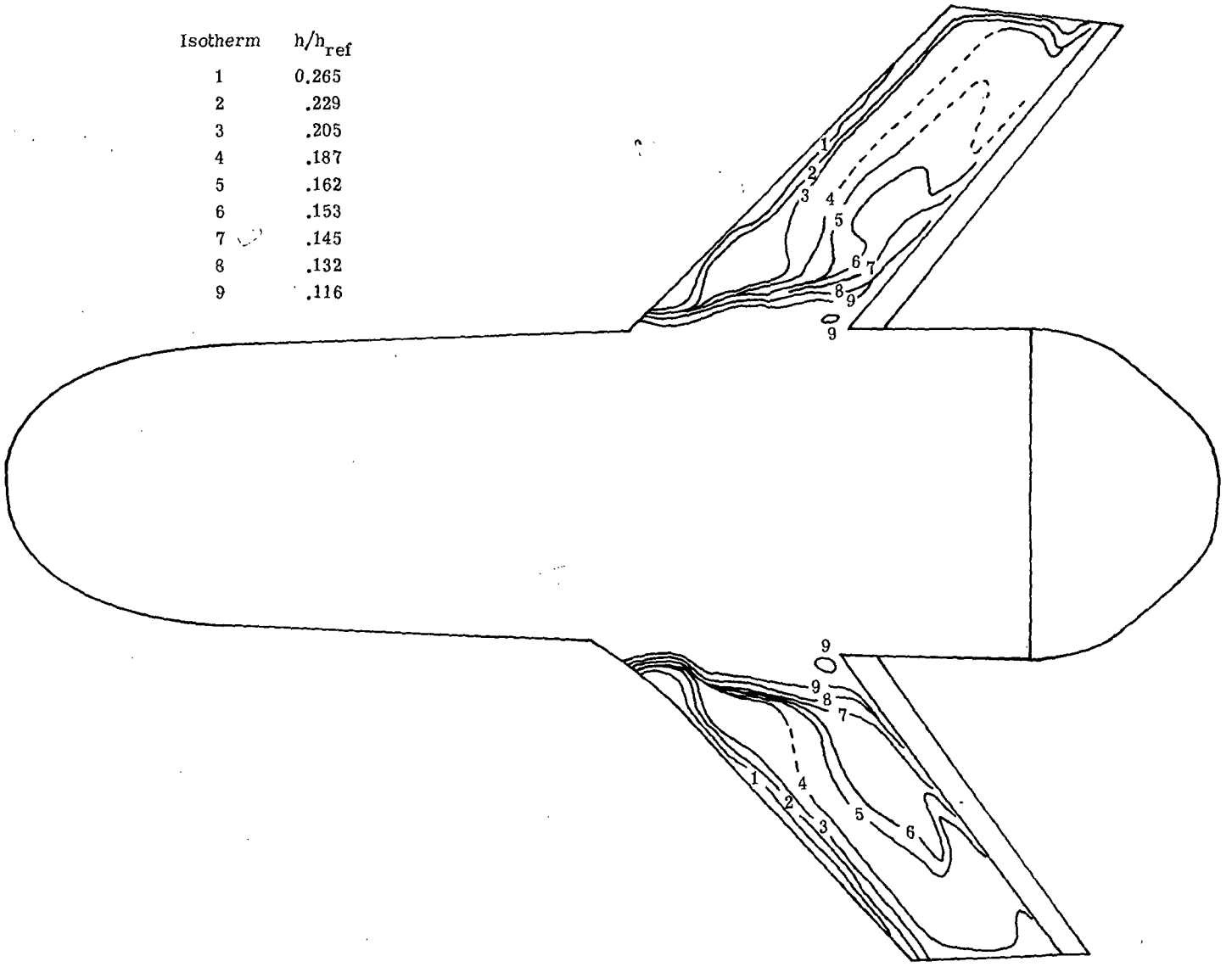

(a) $R_{\infty,\ell} = 0.47 \times 10^6$; $h_{ref} = 619$ W/(m^2-K).

Figure 17.- Heat transfer. $\Lambda = 50^o$; $\alpha = 60^o$.

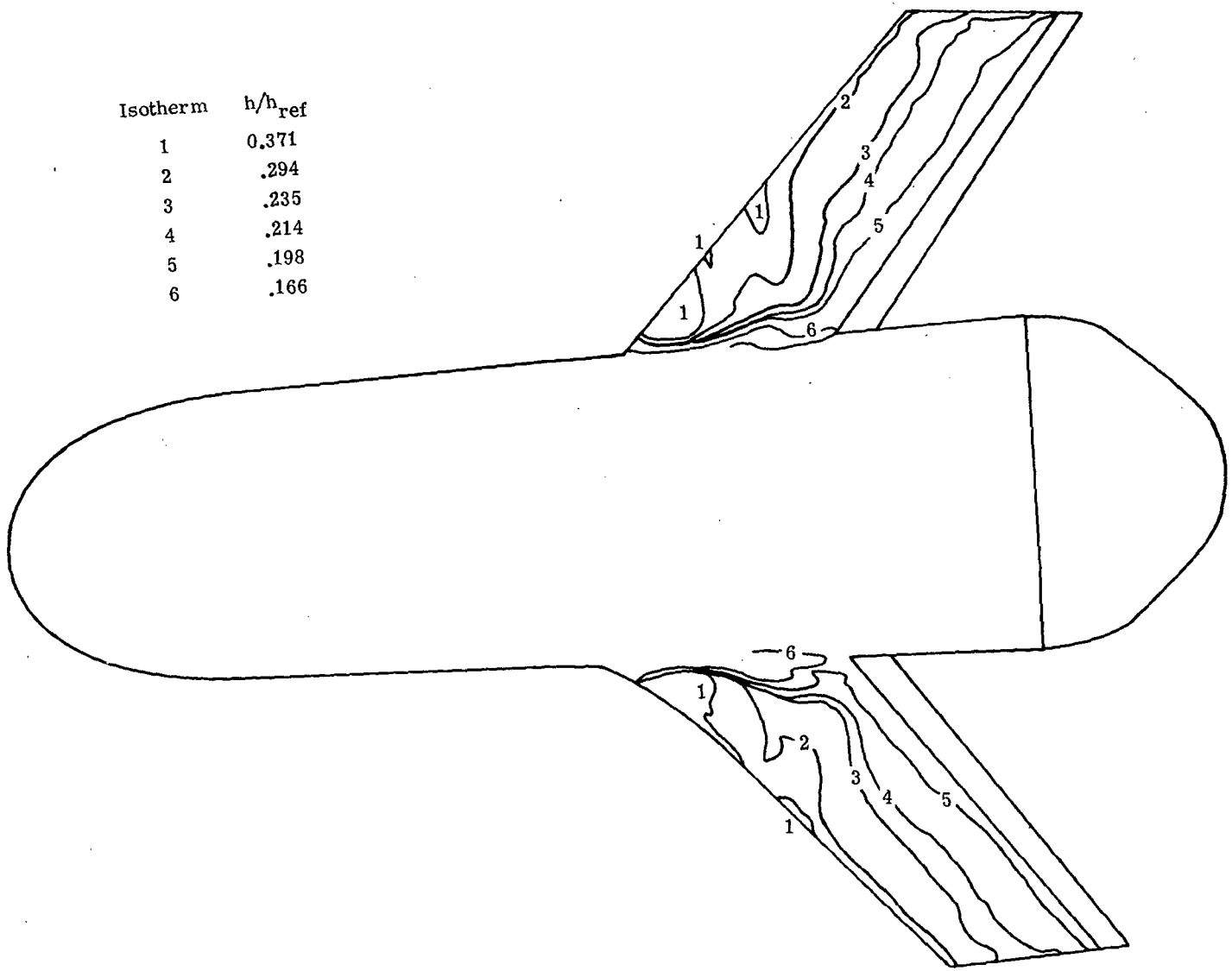

(b) $R_{\infty,\ell} = 1.7 \times 10^6$; $h_{ref} = 1.23$ kW/(m^2-K).

Figure 17.- Concluded.

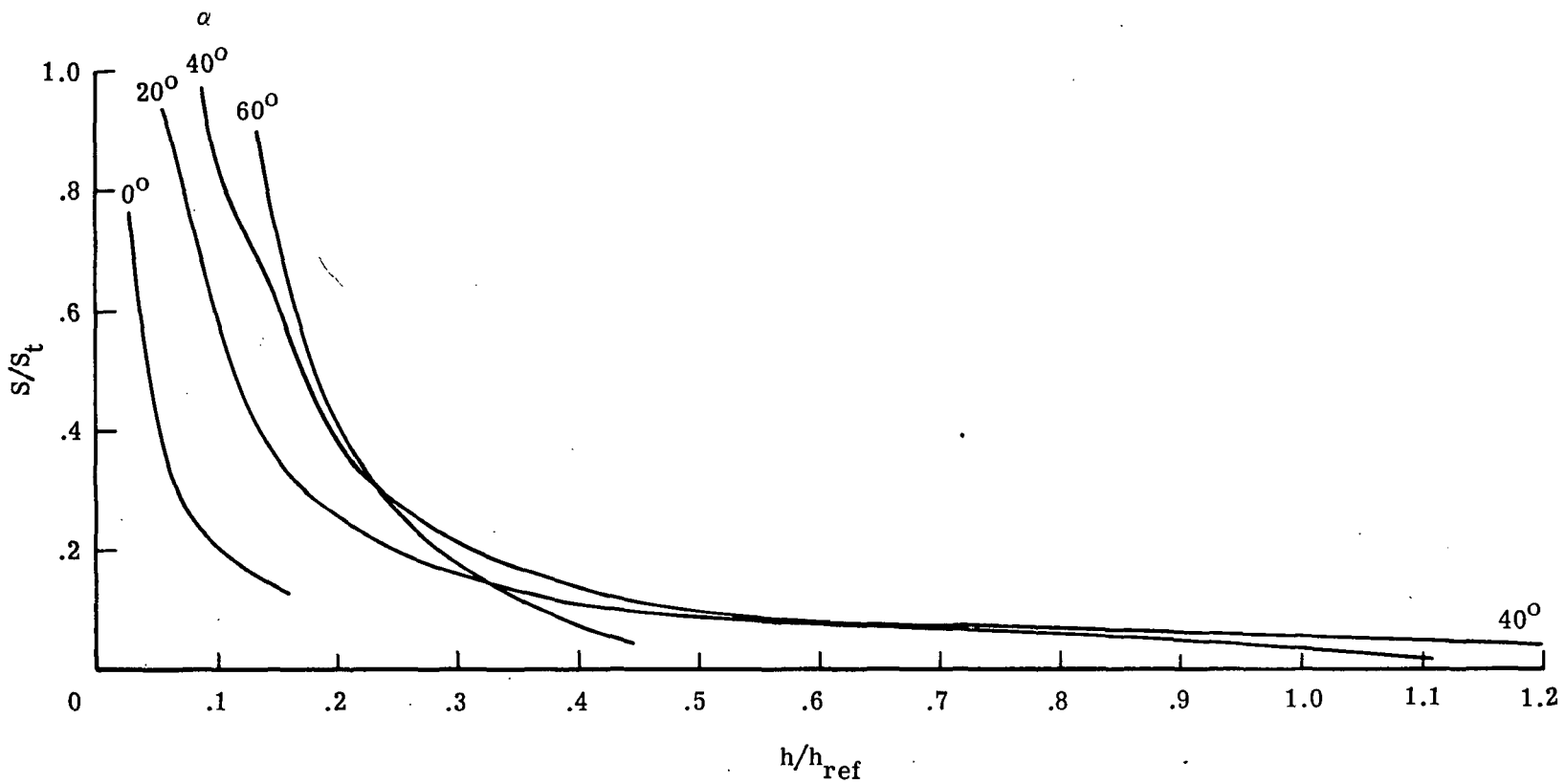

(a) $\Lambda = 14^{o}$.

Figure 18.- Variation of total heating to wing windward surface with angle of attack. $R_{\infty,l} = 0.47 \times 10^{6}$; no wing root fillet.

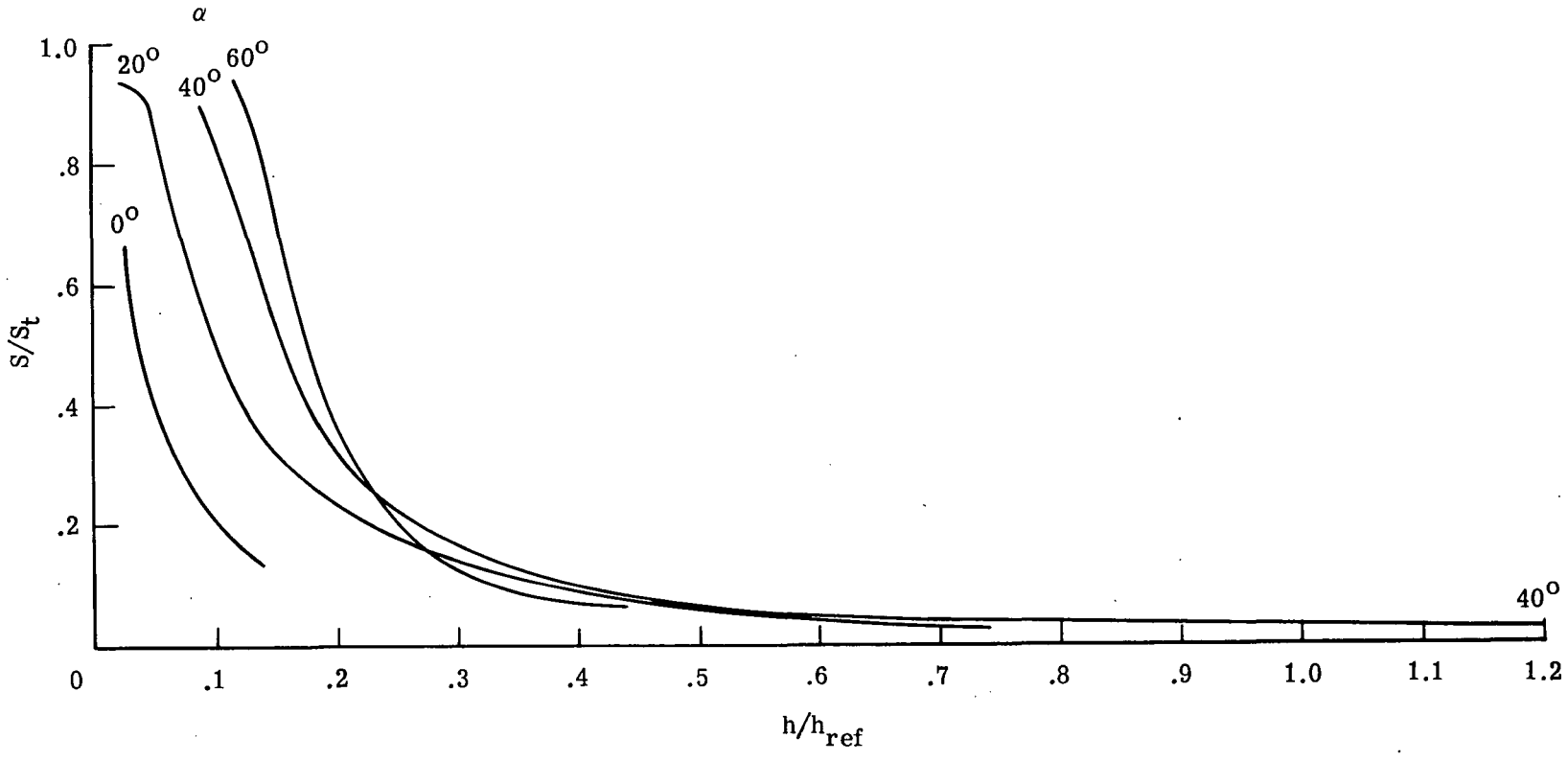

(b) $\Lambda = 25^{o}$.

Figure 18.- Continued.

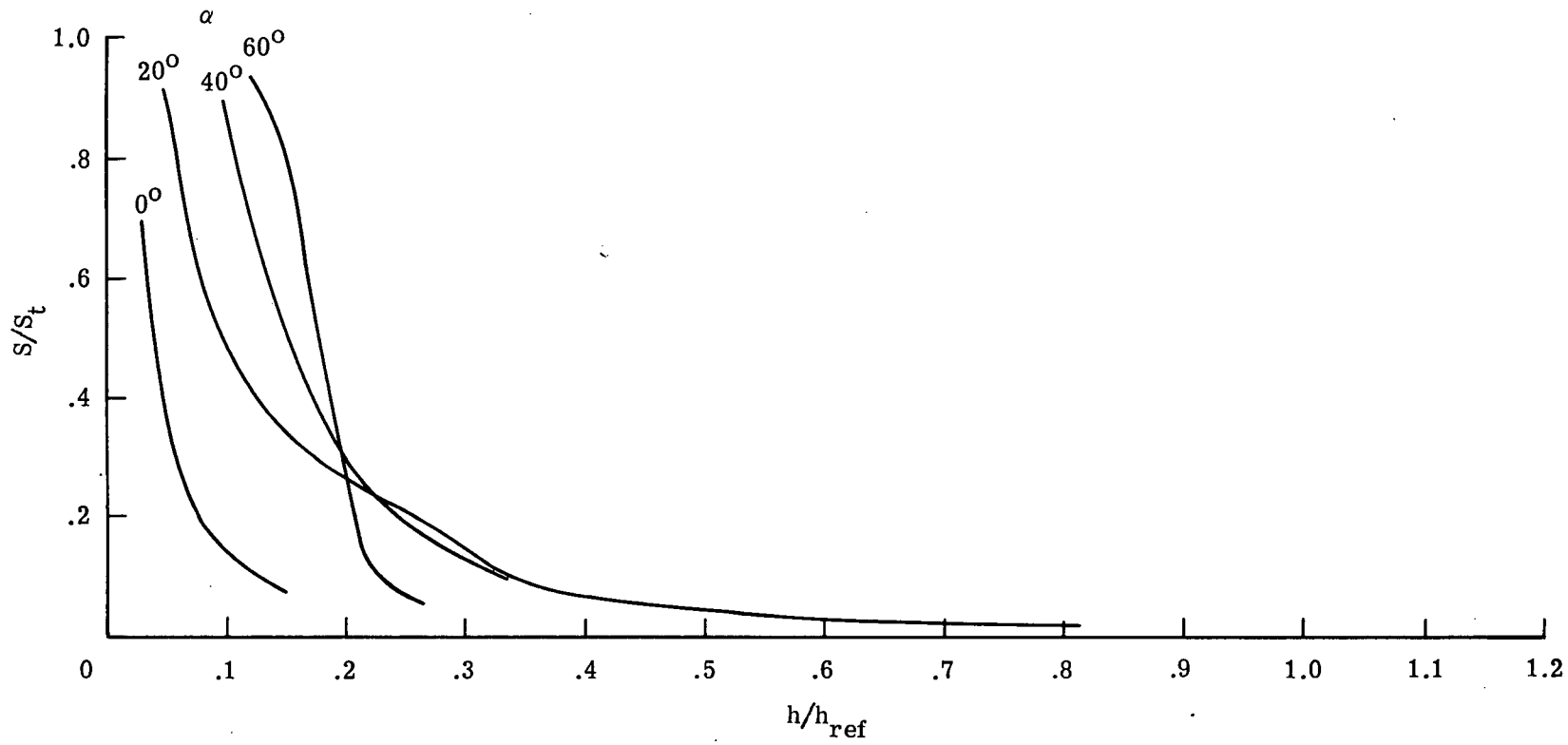

(c) $\Lambda = 50^{\circ}$.

Figure 18.- Concluded.

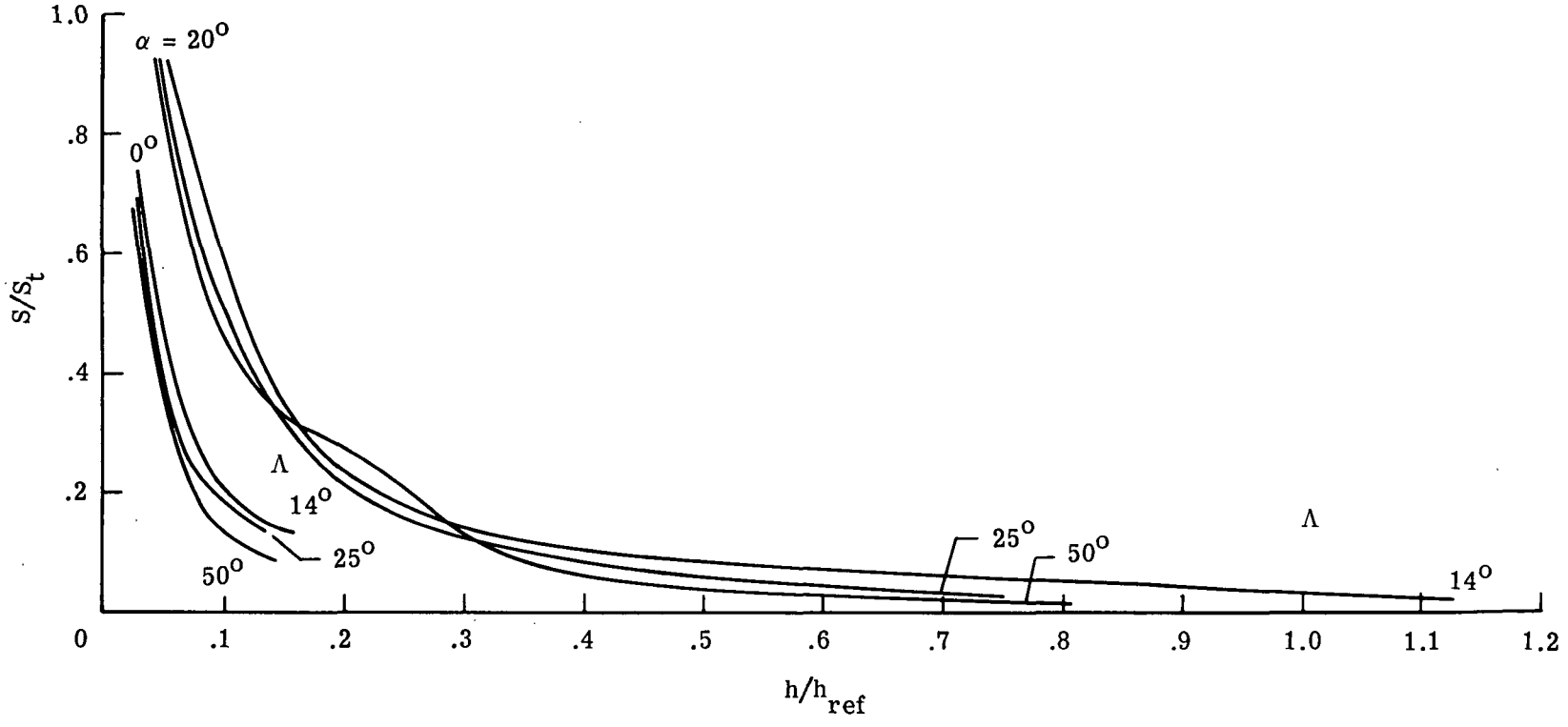

(a) $\alpha = 0^{o}$ and 20^{o}.

Figure 19.- Variation of heating to wing windward surface with leading-edge sweep. $R_{\infty,l} = 0.47 \times 10^{6}$; no wing root fillet.

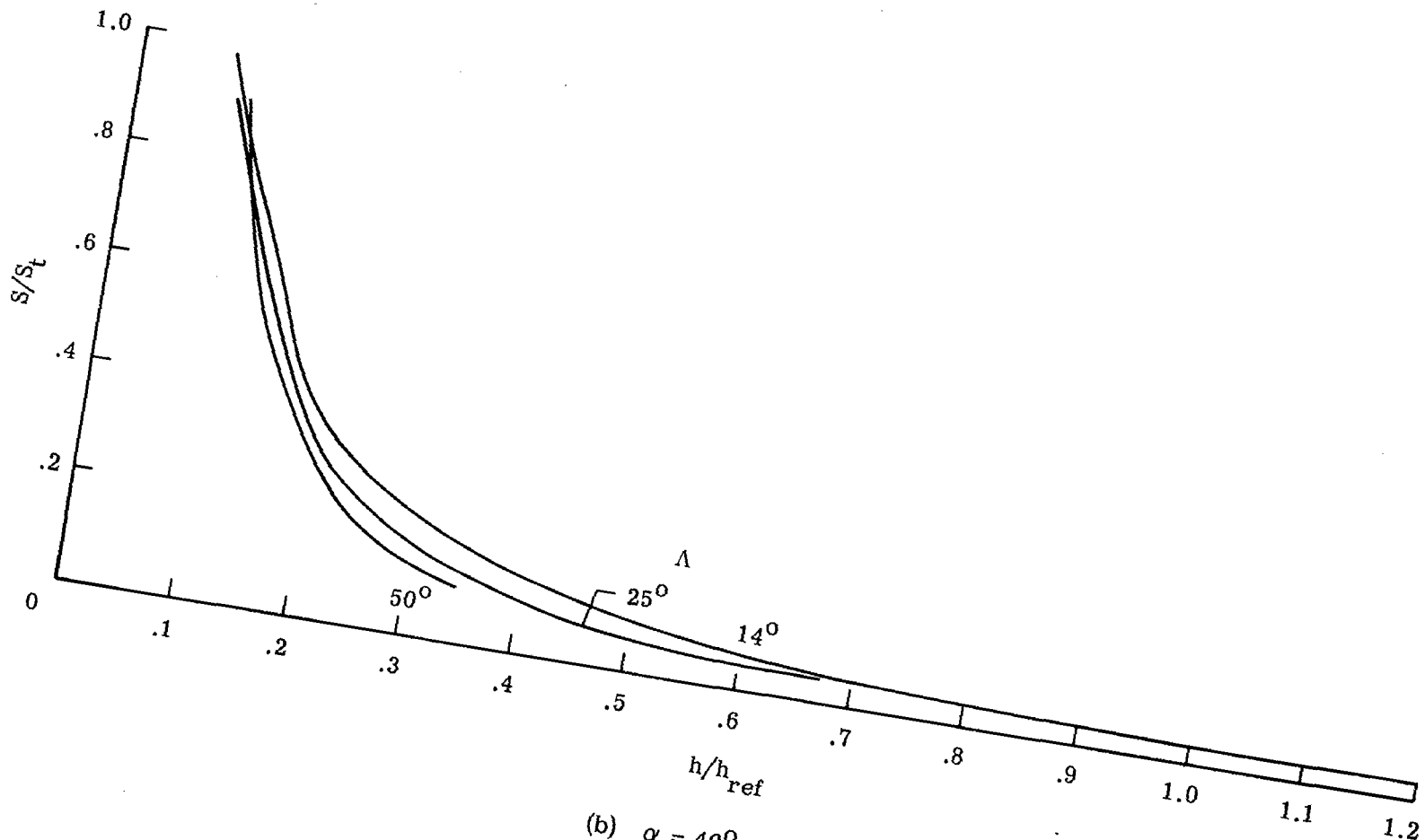

(b) $\alpha = 40°$.

Figure 19.- Continued.

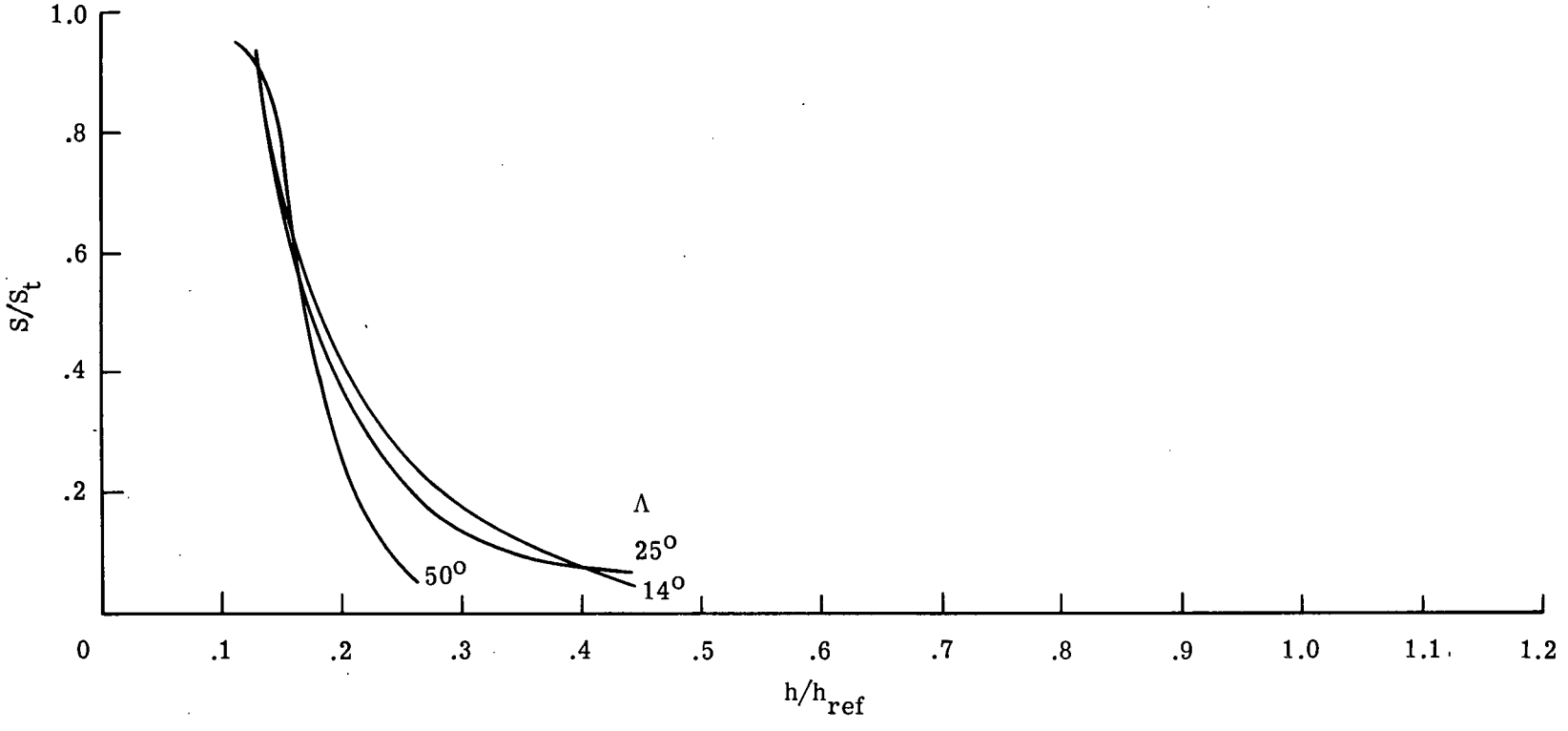

(c) $\alpha = 60^{o}$.

Figure 19.- Concluded.

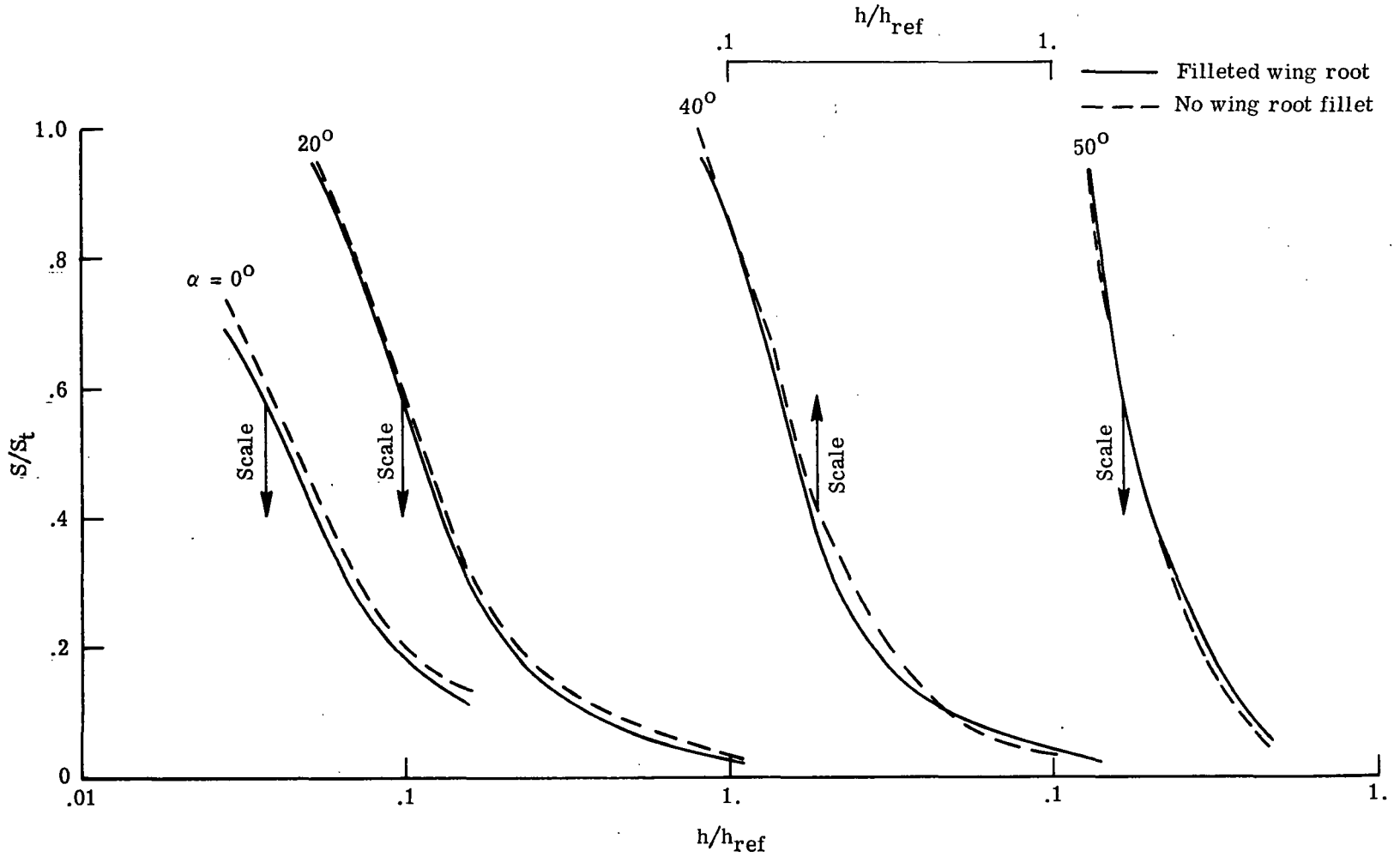

(a) $\Lambda = 14^{\circ}$.

Figure 20.- Effect of wing root fillet on heating to wing windward surface. $R_{\infty,\ell} = 0.47 \times 10^6$.

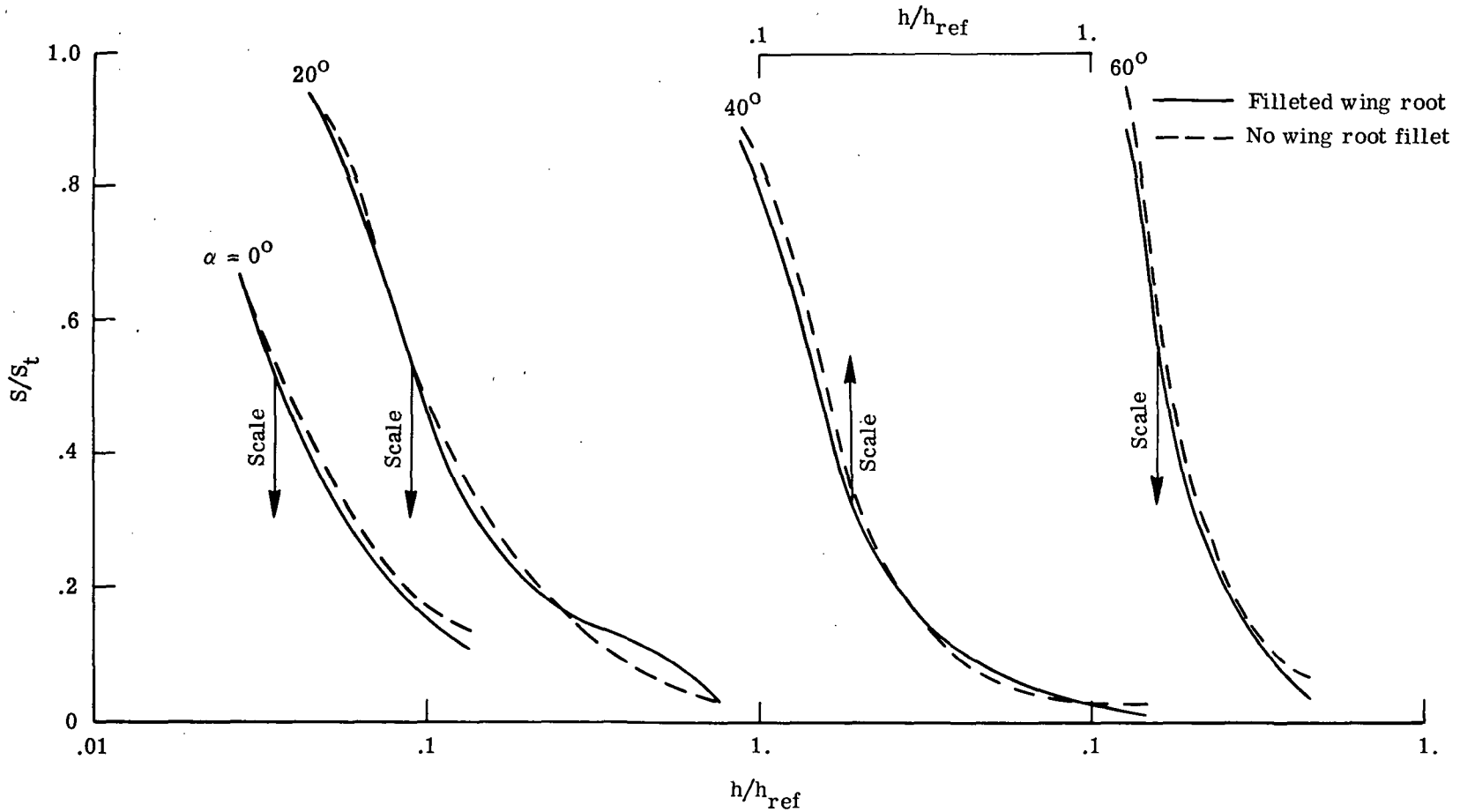

(b) $\Lambda = 25^{\circ}$.

Figure 20.- Continued.

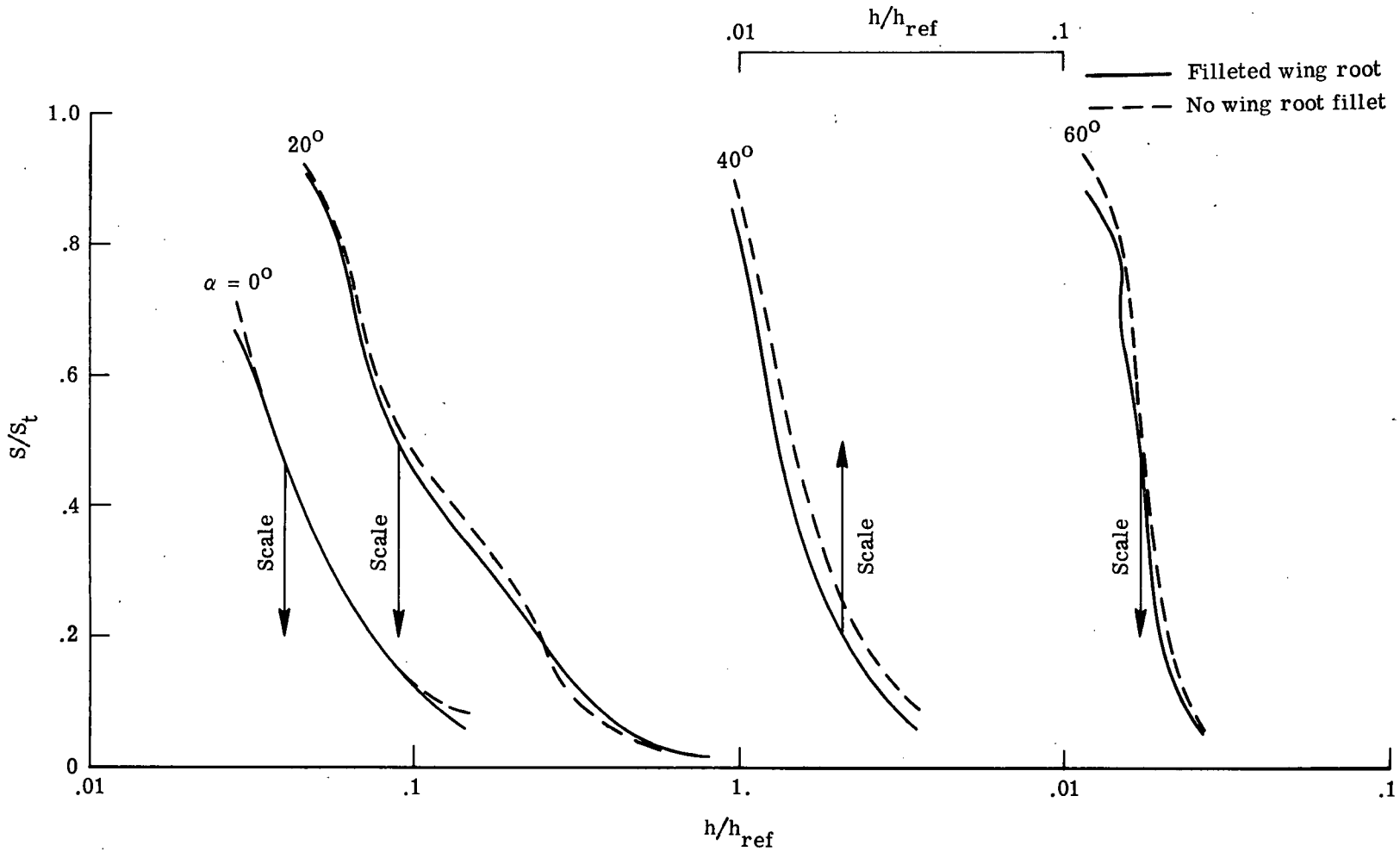

(c) $\Lambda = 50^{o}$.

Figure 20.- Concluded.

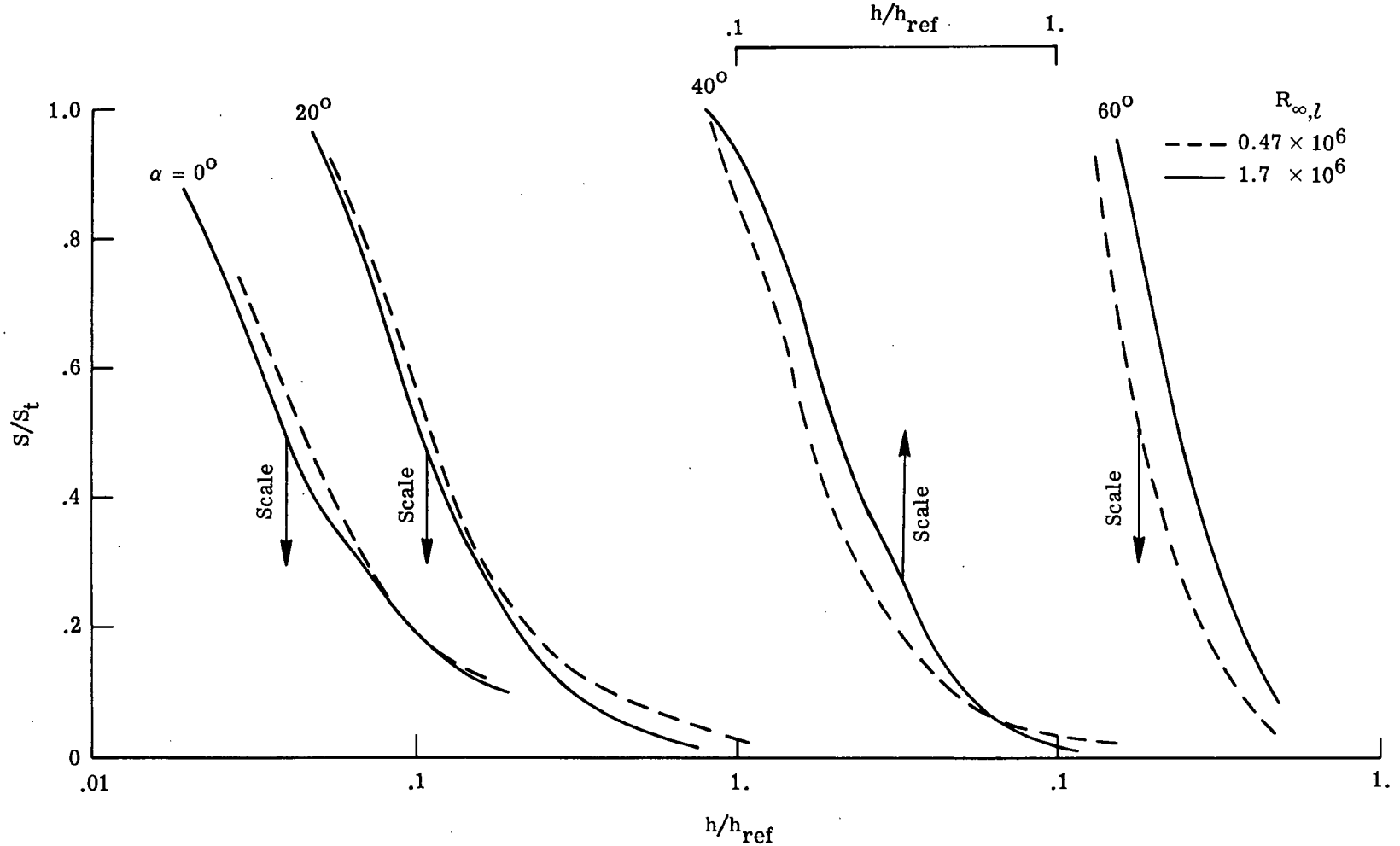

(a) $\Lambda = 14^{\circ}$.

Figure 21.- Effect of Reynolds number on interference heating to wing windward surface.

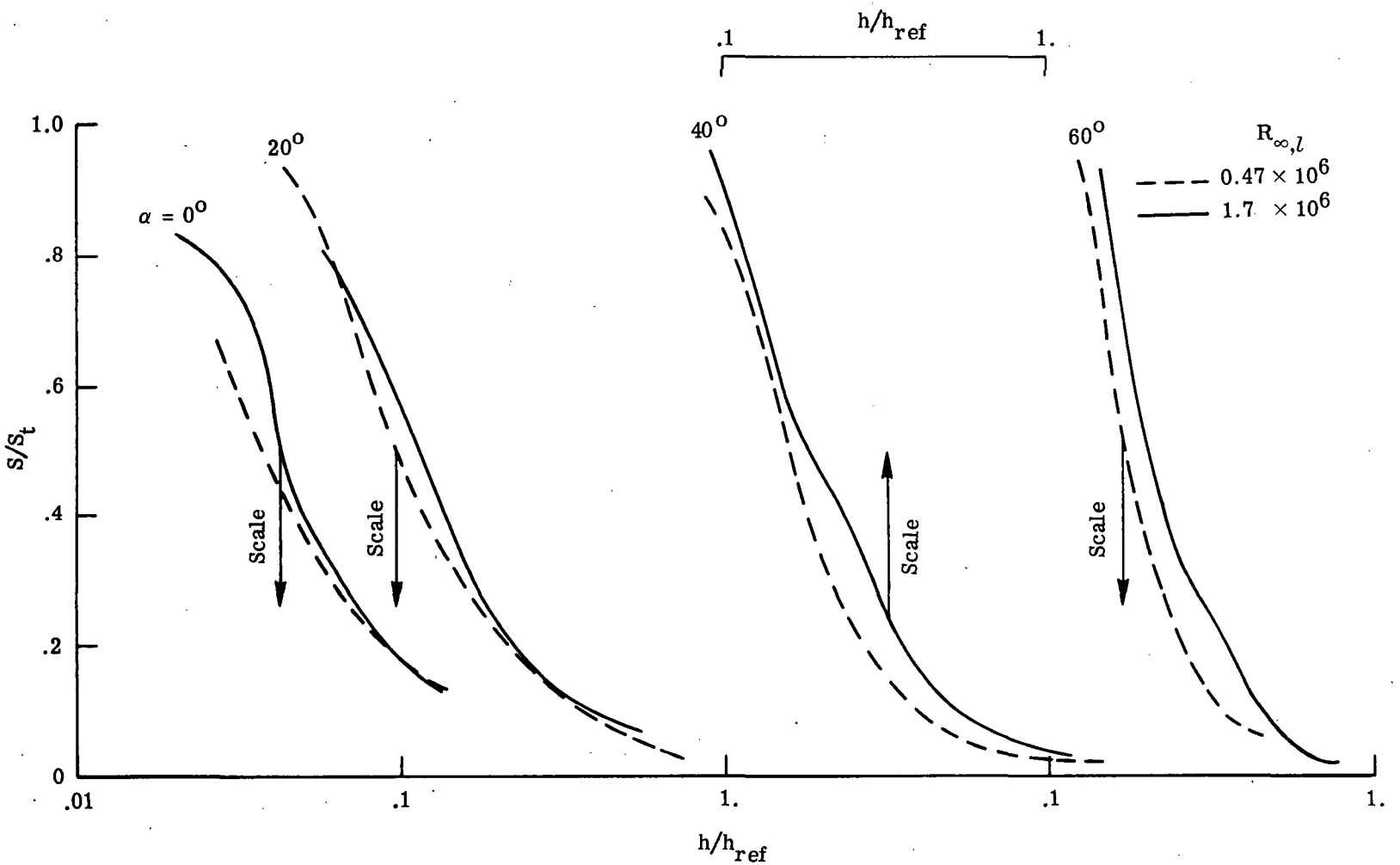

(b) $\Lambda = 25^{\circ}$.

Figure 21.- Continued.

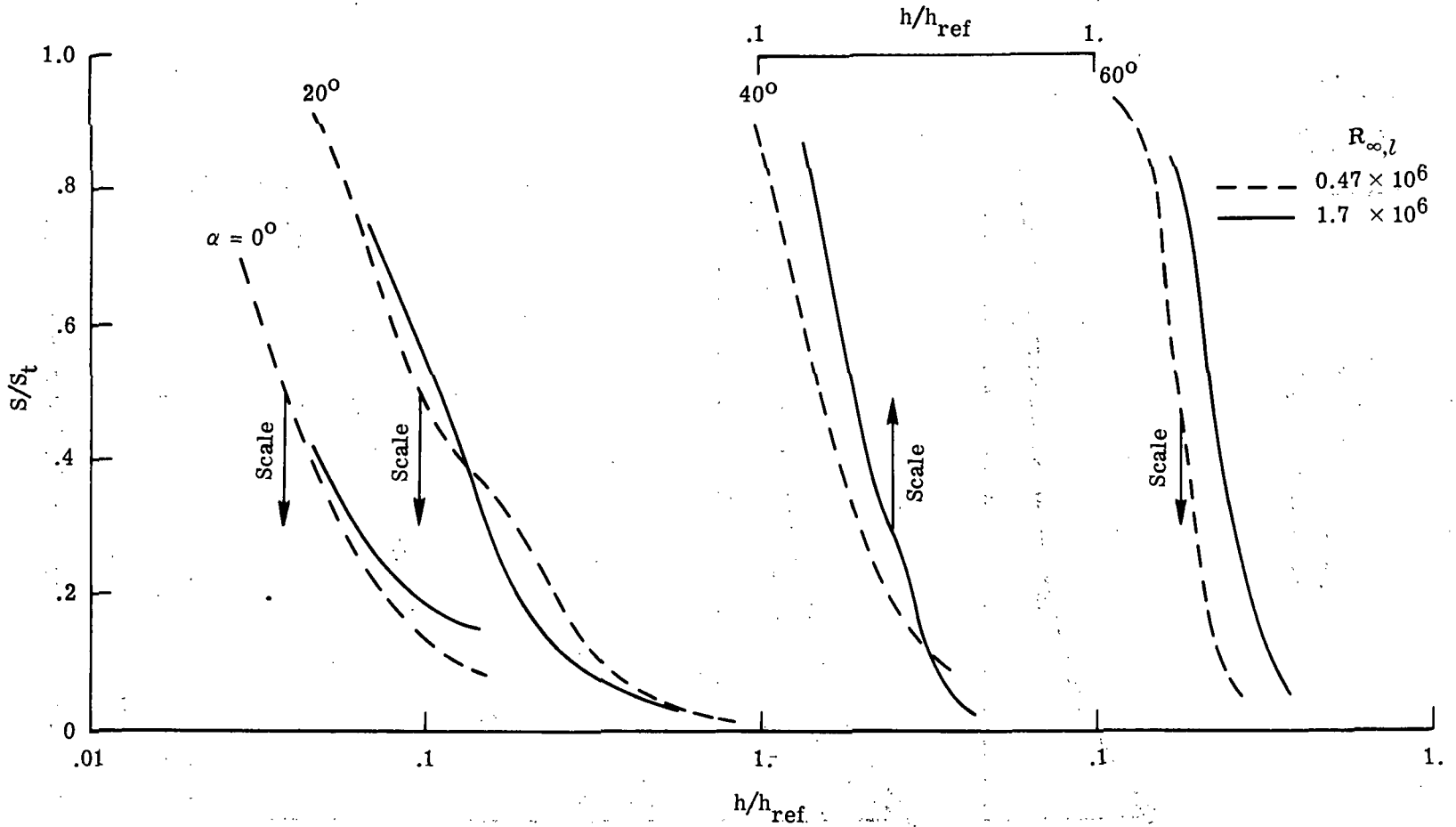

(c) $\Lambda = 50^{\circ}$.

Figure 21.- Concluded.

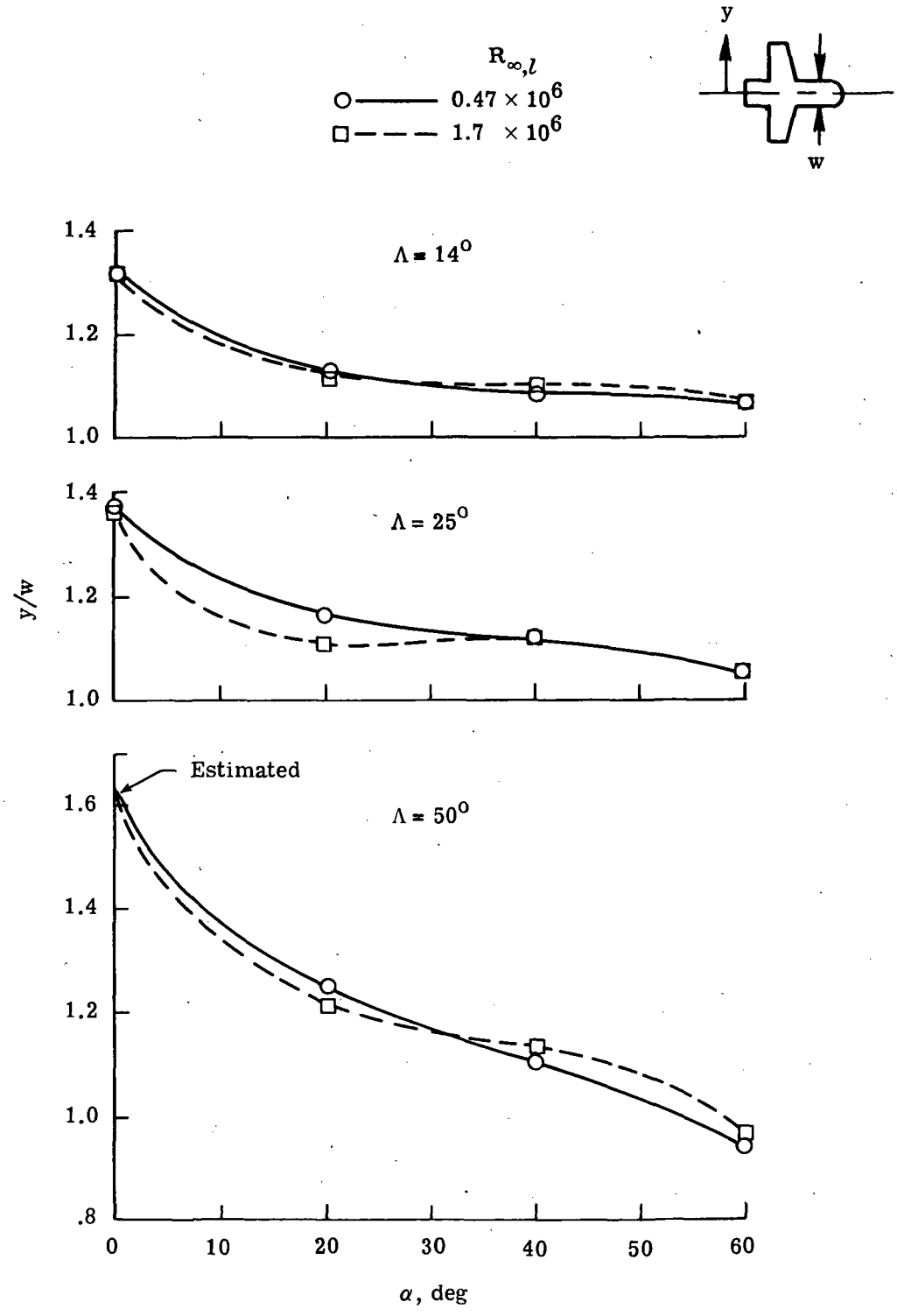

Figure 22.- Transmitted shock impingement point.

NASA-Langley, 1972 — 33 L-8486

NATIONAL AERONAUTICS AND SPACE ADMINISTRATION
WASHINGTON, D.C. 20546

OFFICIAL BUSINESS
PENALTY FOR PRIVATE USE $300

SPECIAL FOURTH-CLASS RATE BOOK

POSTAGE AND FEES PAID
NATIONAL AERONAUTICS AND SPACE ADMINISTRATION
451

U.S.MAIL

POSTMASTER: If Undeliverable (Section 158 Postal Manual) Do Not Return

"The aeronautical and space activities of the United States shall be conducted so as to contribute . . . to the expansion of human knowledge of phenomena in the atmosphere and space. The Administration shall provide for the widest practicable and appropriate dissemination of information concerning its activities and the results thereof."

—NATIONAL AERONAUTICS AND SPACE ACT OF 1958

NASA SCIENTIFIC AND TECHNICAL PUBLICATIONS

TECHNICAL REPORTS: Scientific and technical information considered important, complete, and a lasting contribution to existing knowledge.

TECHNICAL NOTES: Information less broad in scope but nevertheless of importance as a contribution to existing knowledge.

TECHNICAL MEMORANDUMS: Information receiving limited distribution because of preliminary data, security classification, or other reasons. Also includes conference proceedings with either limited or unlimited distribution.

CONTRACTOR REPORTS: Scientific and technical information generated under a NASA contract or grant and considered an important contribution to existing knowledge.

TECHNICAL TRANSLATIONS: Information published in a foreign language considered to merit NASA distribution in English.

SPECIAL PUBLICATIONS: Information derived from or of value to NASA activities. Publications include final reports of major projects, monographs, data compilations, handbooks, sourcebooks, and special bibliographies.

TECHNOLOGY UTILIZATION PUBLICATIONS: Information on technology used by NASA that may be of particular interest in commercial and other non-aerospace applications. Publications include Tech Briefs, Technology Utilization Reports and Technology Surveys.

Details on the availability of these publications may be obtained from:

SCIENTIFIC AND TECHNICAL INFORMATION OFFICE

NATIONAL AERONAUTICS AND SPACE ADMINISTRATION

Washington, D.C. 20546